Marine Pollution Bulletin 189 (2023) 114798

Contents lists available at ScienceDirect

Marine Pollution Bulletin

journal homepage: www.elsevier.com/locate/marpolbul

Decline of anthropogenic lead in South Atlantic Ocean surface waters from 1990 to 2011: New constraints from concentration and isotope data

Arianna Olivelli [a,b,*], Katy Murphy [b], Luke Bridgestock [c], David J. Wilson [b,d], Micha Rijkenberg [e], Rob Middag [e,f], Dominik J. Weiss [b], Tina van de Flierdt [b], Mark Rehkämper [b]

[a] Grantham Institute for Climate Change and the Environment, Imperial College London, South Kensington, London SW7 2AZ, United Kingdom
[b] Department of Earth Science and Engineering, Imperial College London, South Kensington Campus, London SW7 2AZ, United Kingdom
[c] School of Earth and Environmental Sciences, University of St Andrews, Bute Building, Queen's Terrace, St Andrews KY16 9TS, United Kingdom
[d] Department of Earth Sciences, University College London, Gower Place, London WC1E 6BS, United Kingdom
[e] NIOZ Royal Netherlands Institute for Sea Research, Department of Ocean Systems, PO Box 59, 1790 AB Den Burg, the Netherlands
[f] Centre for Isotope Research - Oceans, University of Groningen, PO Box 72, 9700 AB Groningen, the Netherlands

ARTICLE INFO

Keywords:
Lead
Isotopic composition
Seawater
Pollution
GEOTRACES

ABSTRACT

Anthropogenic emissions have severely perturbed the marine biogeochemical cycle of lead (Pb). Here, we present new Pb concentration and isotope data for surface seawater from GEOTRACES section GA02, sampled in the western South Atlantic in 2011. The South Atlantic is divided into three hydrographic zones: *equatorial* (0–20°S), *subtropical* (20–40°S), and *subantarctic* (40–60°S). The equatorial zone is dominated by previously deposited Pb transported by surface currents. The subtropical zone largely reflects anthropogenic Pb emissions from South America, whilst the subantarctic zone presents a mixture of South American anthropogenic Pb and natural Pb from Patagonian dust. The mean Pb concentration of 16.7 ± 3.8 pmol/kg is 34 % lower than in the 1990s, mostly driven by changes in the subtropical zone, with the fraction of natural Pb increasing from 24 % to 36 % between 1996 and 2011. Although anthropogenic Pb remains predominant, these findings demonstrate the effectiveness of policies that banned leaded gasoline.

1. Introduction

Anthropogenic activities have significantly perturbed the biogeochemical cycle of Pb in the last century (Boyle et al., 2014). The combustion of alkyl leaded gasoline was the predominant source of anthropogenic lead pollution to the environment prior to the gradual global phaseout since the late 1970s (Nriagu, 1979; Pacyna and Pacyna, 2001). Only recently, when Algeria banned leaded gasoline in July 2021, was the United Nations Environment Programme able to confirm the complete phaseout of leaded gasoline in all countries of the world (UNEP, 2021). However, numerous other sources of anthropogenic Pb pollution to the environment remain, including high-temperature processes that emit volatile Pb to the atmosphere, such as non-ferrous metal smelting, waste incineration, and coal combustion (Komárek et al., 2008; Nriagu, 1979; Nriagu and Pacyna, 1988; Pacyna and Pacyna, 2001).

The atmosphere, through advection and deposition of aerosols, is the major pathway of anthropogenic Pb to the ocean (Chen et al., 2016; Reuer and Weiss, 2002). As Pb has a relatively short residence time in the atmosphere (<10 days; Niisoe et al., 2010; Reuer and Weiss, 2002) and surface ocean (2–3 years; Bacon et al., 1976; Kadko et al., 2020; Nozaki et al., 1976), it is possible to trace back atmospheric inputs and sources of both anthropogenic and natural Pb in marine surface waters. Such tracing can be achieved by measuring dissolved seawater and particulate Pb isotope compositions and comparing these to the known fingerprints of natural (e.g., dust, rocks) and anthropogenic sources (e.g., lead ores, coal). Lead has four stable isotopes (^{204}Pb, ^{206}Pb, ^{207}Pb, and ^{208}Pb), of which ^{204}Pb is of primordial origin. The other three isotopes are the end products of the radioactive decay of ^{235}U and ^{238}U (to ^{207}Pb and ^{206}Pb, respectively) and ^{232}Th (to ^{208}Pb). The relative abundances of the four Pb isotopes in an ore are therefore determined by the relative concentrations of U, Th, and Pb in the parent rock from which the ore formed and the age of the ore body, giving different Pb ores distinct isotopic fingerprints.

* Corresponding author at: Grantham Institute for Climate Change and the Environment and Department of Earth Science and Engineering, Imperial College London, South Kensington, London SW7 2AZ, United Kingdom.
E-mail address: a.olivelli21@imperial.ac.uk (A. Olivelli).

https://doi.org/10.1016/j.marpolbul.2023.114798
Received 16 December 2022; Received in revised form 27 February 2023; Accepted 1 March 2023
Available online 10 March 2023

Studies of oceanic Pb have mainly focused on the North Atlantic Ocean, which registered the main effects of North American and European emissions from leaded gasoline use in the 20th century. Since the phaseout of alkyl leaded gasoline in North American and Western European countries in the 1970s to 1980s, the Pb concentrations of North Atlantic surface waters have gradually decreased from a peak of ~250 pmol/kg in 1970 to mean levels of ~20 pmol/kg in 2011 (Bridgestock et al., 2016; Kelly et al., 2009; Weiss et al., 2003). These changes demonstrate that environmental and public health policies have been effective in reducing Pb pollution to the atmosphere, and hence the surface ocean. Compared to the North Atlantic, the dissolved Pb concentrations and isotope compositions of seawater in the South Atlantic Ocean have been less well studied, both in terms of spatial coverage and the number of samples analysed (Alleman et al., 2001a; Alleman et al., 2001b; Helmers et al., 1990; Helmers and Rutgers van der Loeff, 1993; Paul et al., 2015a; Paul et al., 2015b; Pohl et al., 1993; Schlosser et al., 2019).

Of the countries surrounding the South Atlantic, only Brazil started with the phaseout of leaded gasoline at around the same time as the phasing out commenced around the North Atlantic (Nriagu et al., 1996; Wolff and Suttie, 1994). Brazil completely phased out leaded petrol in 1991 and Argentina had followed by 1996, whilst this took more than a decade longer in other South American and West African countries (Eichler et al., 2015; Lovei, 1996). In detail, leaded petrol continued to be used in Uruguay until as late as 2004 (Mañay et al., 2008; Queirolo et al., 2010), in Chile until 2005 (Eichler et al., 2015), and in West African countries until 2005 (Todd and Todd, 2010).

In order to investigate the proportion of natural versus anthropogenic Pb in the South Atlantic surface ocean, and to determine the sources of the Pb, we here present total dissolvable Pb concentrations and isotope compositions for surface waters collected in 2011 in a latitudinal transect offshore of the South American coast from Punta Arenas to the equator (Fig. 1).

2. Materials and methods

2.1. Seawater sampling

Twenty-three surface seawater samples were collected in the western South Atlantic during cruise JC057 aboard the *RRS James Cook* from 2nd March to 6th April 2011 (Fig. 1). This cruise formed Leg 3 of the Dutch GEOTRACES GA02 section. Most samples were collected by pumping seawater into a trace-metal clean laboratory from a towed Fish at ~3 m depth, whilst five samples were taken from the topmost bottle (between 9 and 10 m depth) from the ultra-clean CTD (Table 1). After 2 L of seawater had been filled into two pre-cleaned 1 L HDPE bottles, samples were acidified with 2 mL L^{-1} quartz-distilled 6 M HCl, sealed with parafilm, and double bagged. All samples were collected unfiltered, except for two samples which were passed through Sartobran 300 filter capsule filters (0.2 μm). These two samples (sample 5 and sample 21a) were collected at the same time and location as their unfiltered counterparts (sample 4 and sample 20, respectively). Results for filtered

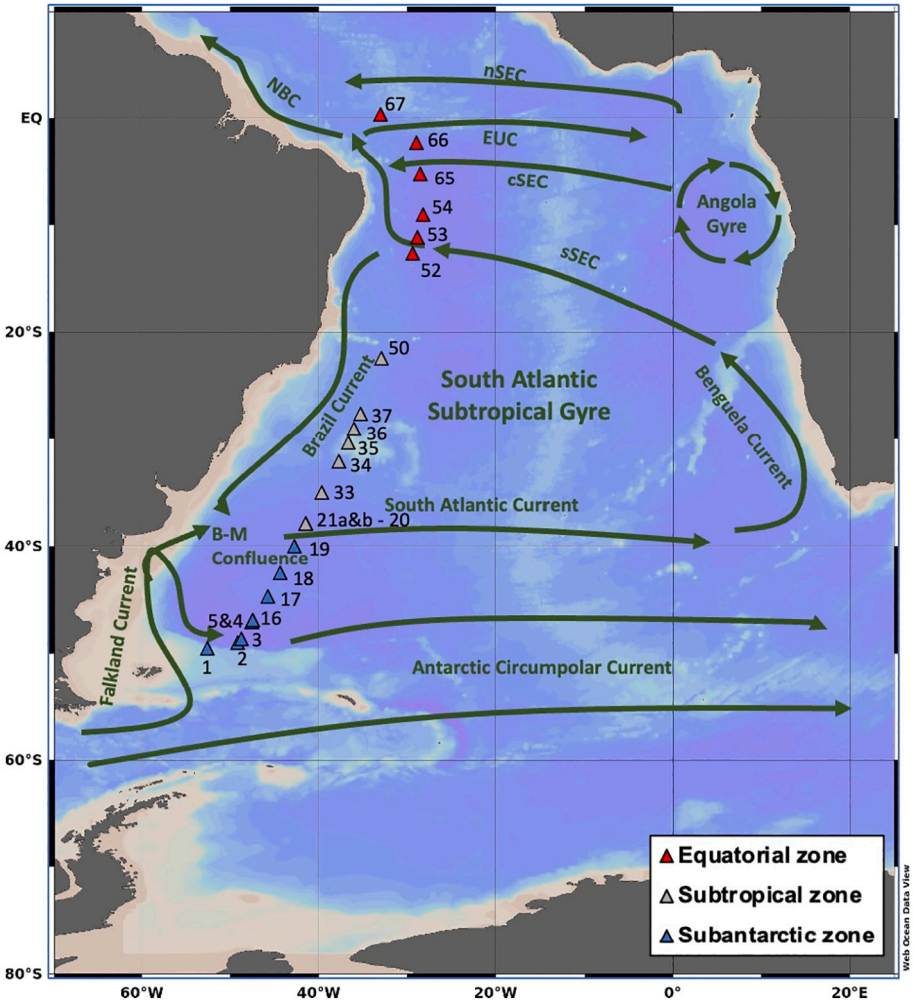

Fig. 1. South Atlantic Ocean surface currents and sampling locations for the GA02 Leg 3 surface waters analysed in this study. Samples are grouped according to oceanographic zones. Abbreviations: NBC – North Brazil Current; EUC – Equatorial Undercurrent; nSEC – northern South Equatorial Current; cSEC – central South Equatorial Current; sSEC – southern South Equatorial Current; B–M Confluence – Brazil-Malvinas Confluence. Map adapted from Peterson and Stramma (1991) and Stramma and England (1999). The conversion between sample numbers and GEOTRACES cast identifiers is available in Table S5.

Table 1
Pb concentrations and isotopic compositions as well as sampling information for the South Atlantic surface water samples analysed in this study. Salinity data obtained from the GEOTRACES Intermediate Data Product Group (2021).

Sample	Sampling information			Water properties		Pb concentration			Pb isotope composition											
	Latitude (°N)	Longitude (°E)	Sample type	Temperature (°C)	Salinity (psu)	[Pb] ± 1 SD (pmol/kg)		n[a]	Sample mass (g)	Pb yield (%)[b]	Pb mass (ng)[c]	$^{206}Pb/^{207}Pb$ ± 2 SD		$^{208}Pb/^{207}Pb$ ± 2 SD		$^{206}Pb/^{204}Pb$ ± 2 SD		$^{207}Pb/^{204}Pb$ ± 2 SD		$^{208}Pb/^{204}Pb$ ± 2 SD	
Subantarctic zone																				
1	−49.489	−52.264	Fish	14.21	34.45	11.7	± 0.6	2	1205	78	2.0	1.16201	± 9	2.43397	± 17	18.1490	± 72	15.6171	± 64	38.014	± 17
2	−48.968	−48.879	CTD	10.12	33.97	9.1	± 0.5	2	1604	80	2.2	1.16115	± 12	2.43331	± 21	18.1130	± 66	15.6000	± 58	37.958	± 14
3[d]	*−48.614*	*−48.459*	*Fish*			*36.7*	± *5.3*	*2*	*1315*	*76*	*6.0*	*1.19533*	± *3*	*2.43503*	± *5*	*18.7787*	± *19*	*15.7098*	± *17*	*38.254*	± *4*
4	−47.074	−47.326	Fish	17.16	34.58	15.3	± 0.1	2	1746	73	3.1	1.18489	± 7	2.43909	± 12	18.5714	± 58	15.6727	± 47	38.229	± 12
5	−47.074	−47.326	Fish[e]	17.16	34.58	13.9	± 0.1	2	1448	76	2.6	1.18397	± 10	2.43858	± 18	18.5607	± 84	15.6783	± 73	38.233	± 18
16	−46.933	−47.220	CTD	17.04	34.62	10.1	± 0.2	3	1840	88	3.3	1.17228	± 4	2.44303	± 8	18.3307	± 38	15.6369	± 35	38.201	± 9
17	−44.702	−45.546	CTD	16.92	34.55	12.5	± 0.0	2	1560	73	2.4	1.17553	± 6	2.44454	± 11	18.3776	± 35	15.6338	± 32	38.216	± 9
18	−42.530	−44.122	Fish	17.91	34.54	14.9	± 0.9	4	1299	74	2.3	1.16794	± 9	2.44036	± 22	18.2388	± 81	15.6172	± 70	38.107	± 18
19	−40.046	−42.539	Fish	21.35	34.55	13.4	± 2.0	5	1219	80	2.4	1.17160	± 7	2.44304	± 12	18.3141	± 60	15.6326	± 50	38.191	± 13
Subtropical zone																				
20	−37.987	−41.221	Fish	20.50	35.48	16.9	± 1.1	3	1468	77	3.2	1.17048	± 10	2.43901	± 17	18.2845	± 60	15.6216	± 58	38.102	± 16
21a	−37.987	−41.221	Fish[e]	20.50	35.48	16.9	± 0.3	2	843	94	2.8	1.17129	± 7	2.44035	± 12	18.3102	± 49	15.6324	± 43	38.148	± 11
21b[d]	*−37.987*	*−41.221*	*Fish*[e]			*24.5*	± *1.2*	*2*	*474*	*88*	*2.0*	*1.13555*	± *12*	*2.40626*	± *25*	*17.7047*	± *137*	*15.5916*	± *112*	*37.519*	± *28*
33	−35.123	−39.501	Fish	22.01	35.73	21.3	± 0.3	4	1304	80	3.9	1.17151	± 7	2.43746	± 13	18.3247	± 43	15.6418	± 39	38.126	± 10
34	−32.278	−37.590	Fish	24.00	36.14	21.9	± 0.2	2	1487	86	5.3	1.17199	± 6	2.43790	± 9	18.3305	± 31	15.6411	± 30	38.131	± 7
35	−30.471	−36.550	Fish	23.76	35.58	21.0	± 0.6	3	1284	95	5.4	1.16963	± 5	2.43600	± 9	18.2423	± 49	15.5964	± 43	37.994	± 11
36	−29.224	−35.868	Fish	24.61	35.58	21.3	± 0.6	2	1235	75	3.2	1.17024	± 6	2.43658	± 10	18.2973	± 42	15.6357	± 39	38.099	± 10
37	−27.827	−35.145	Fish	25.93	36.54	18.9	± 0.8	4	1271	91	4.4	1.17144	± 7	2.43872	± 10	18.3326	± 58	15.6517	± 49	38.169	± 12
50	−22.753	−32.841	Fish	26.44	36.58	21.2	± 0.5	2	1276	75	3.3	1.16431	± 11	2.43505	± 18	18.1924	± 99	15.6263	± 89	38.051	± 22
Equatorial zone																				
52	−13.011	−29.259	Fish	28.32	37.10	16.4	± 0.0	2	1306	75	2.7	1.16402	± 5	2.44032	± 9	18.1834	± 41	15.6209	± 37	38.120	± 9
53	−11.514	−28.765	Fish	28.93	36.98	15.8	± 0.4	2	1736	75	3.4	1.16449	± 5	2.44081	± 8	18.2171	± 38	15.6436	± 33	38.183	± 8
54	−9.487	−28.106	Fish	28.86	36.84	16.1	± 0.8	2	1729	85	4.5	1.16455	± 4	2.44116	± 8	18.2120	± 42	15.6391	± 37	38.176	± 9
65	−5.677	−28.460	CTD	28.88	36.28	19.0	± 0.6	2	1806	89	6.0	1.17078	± 6	2.44559	± 11	18.3100	± 33	15.6398	± 28	38.247	± 8
66	−2.803	−28.884	Fish		35.57	20.5	± 0.6	2	1574	85	5.1	1.16436	± 5	2.44185	± 8	18.1941	± 32	15.6255	± 28	38.155	± 7
67	−0.183	−32.882	CTD	28.53	35.71	18.9	± 0.2	2	1757	91	6.0	1.16777	± 5	2.44457	± 10	18.2623	± 29	15.6388	± 25	38.231	± 6
Mean						16.7			1454	82	3.6	1.16983		2.43961		18.2886		15.6338		38.140	
1SD for [Pb]/2SD for Pb isotopes						3.8			254	7	1.4	0.01217		0.00680		0.2252		0.0382		0.161	

[a] Number of individual sample aliquots analysed for determination of Pb concentration.
[b] Percentage recovery of Pb during isotope composition procedure.
[c] Mass of Pb available for isotope composition measurement.
[d] Sample disregarded in the discussion due to possible Pb contamination.
[e] Filtered sample.

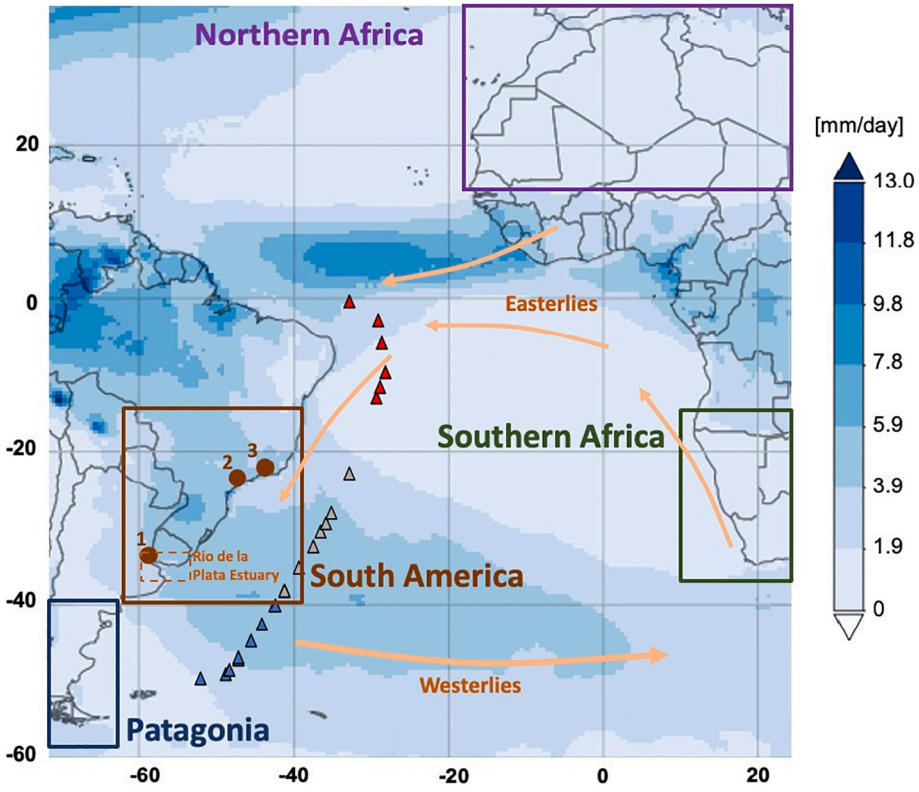

Fig. 2. Map of average annual precipitation (mm/day) from 2000 to 2020 (blue colour shading; data from GPCP Version 3.1 Daily Precipitation Data Set) and predominant wind directions in the South Atlantic Ocean (orange arrows, adapted from the NCEP/NCAR Reanalysis product; Kalnay et al., 1996). The four boxes represent the four major source areas that may provide natural and anthropogenic Pb to western South Atlantic Ocean surface waters and for which Pb isotope data are available in the literature (see text for details). Points 1, 2, and 3 represent Buenos Aires, Saõ Paulo, and Rio de Janeiro, respectively. Triangles mark the locations of the surface water samples analysed in this study (colours match the legend in Fig. 1). (For interpretation of the references to colour in this figure legend, the reader is referred to the web version of this article.)

samples will be referred to as "dissolved", and results for unfiltered samples will be referred to as "total dissolvable", following GEOTRACES parameter-naming conventions.

2.2. Hydrography and wind patterns of the sampling region

Annual wind patterns north of 30°S in the South Atlantic are dominated by the south-east trade winds (Fig. 2). These winds blow towards the equator and meet the north-east trade winds at the intertropical convergence zone (ITCZ). The ITCZ is at its furthest north (9°N) during the Northern Hemisphere summer and furthest south (2°N) during the Northern Hemisphere winter (Schneider et al., 2014). The location of the ITCZ controls a band of intense rainfall (over 3000 mm/yr; Huffman et al., 2021; Fig. 2) in the tropics, which stands in contrast to the desert-like levels of precipitation in the region of the south-east trade winds that characterise most of the eastern subtropical South Atlantic. Another area of intense rainfall is located in the western subtropical South Atlantic (up to ~2500 mm/yr; Huffman et al., 2021; Fig. 2). Here, the South Atlantic Convergence Zone (SACZ) manifests as a NW-SE orientated belt of precipitation that extends from the Amazon basin to the subtropical South Atlantic. The SACZ is at its greatest extent during the Southern Hemisphere summer (Bombardi et al., 2014; Kodama, 1993). Areas of intense rainfall are relevant for atmosphere-ocean Pb cycling because precipitation removes the majority of aerosol dust loads, thus contributing to the deposition of trace metals in the surface ocean. South of 40°S, the predominant winds are westerlies, which increase in strength eastwards (Fig. 2).

Annually averaged dust deposition fluxes in the South Atlantic Ocean vary between 0.05 and 10 g m^{-2} yr^{-1}(Kok et al., 2021). They are higher than 1 g m^{-2} yr^{-1} off the coast of South America between 30° and 60°S, where a dust plume driven by the westerly winds extends towards the centre of the basin, and off the coast of western Africa between 10° and 30°S. Fluxes from the North African dust plume are above 1 g m^{-2} yr^{-1} only at low latitudes near the equator (<5°S). As such, the dust fluxes in the South Atlantic Ocean are significantly lower than the fluxes observed in the North Atlantic basin, which reach up to 50 g m^{-2} yr^{-1} (Kok et al., 2021).

Surface water circulation in the South Atlantic has a similar pattern to the lower tropospheric circulation summarised above. Broadly, it comprises mainly east-west (but also some west-east) equatorial currents in the northern section of the basin, the counter-clockwise flow of the South Atlantic Subtropical Gyre (SASG) between ~20 and 40°S, and the eastward-flowing Antarctic Circumpolar Current south of 40°S (Fig. 1). The counter-clockwise flow of the SASG is very slow in the centre, with a faster-flowing western boundary current known as the Brazil Current (BC). The Brazil Current flows southwards along the Brazilian coast, where it meets the northward flowing Falkland (or Malvinas) Current, marking the Brazil-Malvinas Confluence, before deflecting eastwards along the Subtropical Front at about 40°S and feeding the South Atlantic Current (SAC; Stramma and England, 1999). Near southern Africa, a portion of the SAC turns northwards to feed the Benguela Current, which is the eastern boundary current of the SASG (Stramma and Peterson, 1990). The Benguela Current then feeds the broad, sluggish South Equatorial Current (SEC) which flows in a westerly/north-westerly direction (Peterson and Stramma, 1991; Stramma and England, 1999). At the easternmost point of South America, the SEC splits into two parts: the north-westward flowing North Brazil Current (NBC), and the aforementioned Brazil Current (Lumpkin and Garzoli, 2005; Stramma and England, 1999).

The SEC comprises southern, central, and northern branches, abbreviated as sSEC, cSEC and nSEC, respectively (Fig. 1; Lumpkin and Garzoli, 2005). The sSEC (about 8 to 20°S) flows in a north-westward/westward direction across the South Atlantic until it approaches 30°W and turns south-westwards, eventually splitting into two branches, one feeding the southward-flowing BC and the other flowing northward and feeding the NBC (Fig. 1; Lumpkin and Garzoli, 2005). The cSEC (about 4 to 8°S) and nSEC (about 0 to 4°N) are indistinguishable from each other east of 5°W, but by 20°W there are two distinct currents which go on to feed into the NBC (Bourlès et al., 1999; Lumpkin and Garzoli, 2005). Finally, the Equatorial Undercurrent (EUC; 2°S – 3°N), located between

the cSEC and nSEC, flows in an eastward direction. It is formed by a tight retroflection of the NBC at the equator and has its velocity core at about 100 m depth (Bourlès et al., 1999; Rosell-Fieschi et al., 2015). However, during the Northern Hemisphere spring, it speeds up and shoals to reach shallower depths (Brandt et al., 2006; Rosell-Fieschi et al., 2015; Urbano et al., 2008).

2.3. Analytical techniques

All post-cruise work was conducted in ISO class 4 laminar flow hoods in an ISO class 6 clean room, and in mass spectrometer laboratories at Imperial College London. The water used was of 18.2 MΩ cm quality from a Millipore Milli-Q Academic system. Nitric, hydrochloric, and hydrofluoric acids were distilled in-house using Teflon or quartz stills, and Suprapur or Optima grade hydrobromic acid was purchased from Merck or Fisher Chemical. The purified acids had a maximum Pb concentration of 4 pg mL^{-1}. Aqueous ammonia solutions of about 9 M were prepared from VWR AnalaR ammonia solution by cold vapour equilibration with water in a Teflon elbow for one week. All required acid mixtures were prepared on the day of use.

2.3.1. Determination of Pb isotope compositions

The employed methods were largely the same as the procedures described by Paul et al. (2015a). In brief, Pb isotope compositions were determined by pre-concentrating the Pb from about 1.5 L of seawater by the addition of ammonia solution until a $Mg(OH)_2$ precipitate formed in a Teflon separating funnel (Weiss et al., 2000). This precipitate was collected, rinsed with water to remove salt, and dissolved in 2 M HBr – 0.01 M HF in preparation for Pb purification by anion exchange chromatography. Samples were left overnight with lids loose to allow any gases produced by reactions involving residual organics to escape, to avoid the formation of gas bubbles in the resin bed. The anion exchange chromatography used Biorad AG1-X8 100–200 mesh resin and mixtures of dilute HNO_3, HF, and HBr, as detailed in Table S1. The procedure was repeated to further purify the Pb, and the final eluted Pb was split in two parts. One third of the solution was spiked with a ^{204}Pb-^{207}Pb double spike, whilst the remaining two thirds of the solution was left unspiked (Paul et al., 2015a).

Lead solutions were dried and loaded in 2 M HNO_3 onto Re filaments with silica gel activator. The filaments were then baked for 3 h in the source of a Thermo Finnigan Triton thermal ionisation mass spectrometer (TIMS). The Pb isotope measurements were carried out at typical filament temperatures of ~1300 °C, using Faraday cups with 10^{11} Ω resistors for all Pb isotopes and interfering elements, except for unspiked analyses, where the ^{204}Pb ion beam was monitored using a 10^{12} Ω resistor (Wilson et al., 2017). Data were collected in 15 blocks of 15 cycles of 8.3 s, with baseline measurements before each block. A peak centring procedure was carried out before the first measurement block. To correct for mass bias, the measured data for spiked and unspiked runs of each sample were processed using an iterative double spike data reduction routine, as described by Rudge et al. (2009).

2.3.2. Determination of Pb concentrations

Lead concentrations were determined by isotope dilution (ID) following the method described by Paul et al. (2015a). In brief, the same ^{204}Pb-^{207}Pb double spike was added to 50 mL aliquots of the seawater samples and allowed to equilibrate for at least ten days. Ammonia solution was added, causing co-precipitation of Pb with $Mg(OH)_2$, and the resulting precipitate was separated from the supernatant by centrifugation. The precipitate was then dissolved in the column-loading solution in preparation for a shortened version of the anion exchange procedure (Table S2). Samples were prepared for TIMS analyses as described above. Depending on the amount of Pb available for analysis and the ion beam intensity initially observed, TIMS measurements employed Faraday cups using five blocks of 15 cycles, or a secondary electron multiplier coupled to an ion counting system in four blocks of 20 cycles with peak hopping between the four Pb isotopes and a baseline measurement before each block. To calculate Pb concentrations using standard ID techniques, the raw isotope ratio data were processed offline using the previously determined isotope compositions of the sample and the double spike.

The Pb concentration of each sample was determined at least twice on separate seawater aliquots, to ensure the two available 1 L bottles for each seawater sample were assessed separately. This approach enabled spuriously high blanks to be identified, and such results were discarded.

2.3.3. Blank contribution and data quality

Monitoring blank contributions to samples is particularly important for marine Pb studies, as very small quantities of the element are often processed and there are many opportunities for contamination. This is especially true for concentration measurements, since only ~190 pg of natural Pb were processed for each sample. Two blanks were included in each batch of six to ten samples processed for the determination of Pb concentrations. The first blank was a "procedural blank", where 0.1 mL seawater (with <0.5 pg Pb) was processed following the usual procedure, yielding a mean blank of 23 ± 10 pg Pb (1 SD, n = 14). The second blank was a "reagent blank", where the ammonia solution and double spike were first dried down, and the usual procedure was then followed, which yielded a mean blank of 15 ± 9 pg Pb (1 SD, n = 11). Both types of blanks were essentially identical, and accordingly all Pb concentrations were corrected for a mean blank contribution of 20 pg Pb. This correction is equivalent to about 12 % of the original natural Pb in a typical 50 mL aliquot of a surface seawater sample in the South Atlantic Ocean.

For the isotope composition measurements, one blank was processed per batch of three samples. As for the "reagent blank" described above, there was no seawater involved; instead, the ammonia solution was added to the separating funnel, removed and dried, and the chemical separation procedure was then followed as normal. Despite the much larger reagent volumes involved, the mean blank was similar to the ID blank at 24 ± 11 pg Pb (1 SD, n = 12). In comparison, the mean mass of Pb available for isotope composition measurements on a sample was 3.6 ± 1.4 ng (1 SD, n = 24), given that the procedure for the chemical separation and purification of Pb had a mean yield of 82 ± 7 % (1 SD, n = 24). Hence, the blank contribution is equivalent to ~0.7 % of the Pb present in the surface seawater samples analysed for Pb isotope compositions. This contribution is nearly negligible, and the isotope composition of the blank was not well defined, so no blank corrections were applied to the Pb isotope data.

To assess long-term reproducibility, repeat analyses of 2 and 10 ng of the NIST standard reference material (SRM) 981 Pb were carried out during the sample analysis period of nine months. Furthermore, four aliquots of the GEOTRACES intercalibration sample GSP were analysed during the same period. The results obtained for the SRM 981 Pb analyses are in good agreement with published values (Table S3; Galer and Abouchami, 1998; Klaver et al., 2016; Paul et al., 2015a; Wilson et al., 2017). For 10 ng Pb loads, the within-run precision (2 SE) was about ± 80 ppm ($^{20x}Pb/^{204}Pb$) or ± 20 ppm ($^{206}Pb/^{207}Pb$, $^{208}Pb/^{207}Pb$), whilst for 2 ng Pb loads the precision was about a factor of two worse at about ± 200 ppm and ± 40 ppm, respectively. The analyses of the four GSP sample aliquots, with about 11 ng Pb and 91 % yield, gave a Pb concentration of 56.3 ± 1.7 pmol/kg (1 SD, n = 4) and Pb isotope ratios ($^{206}Pb/^{207}Pb = 1.158 \pm 0.014$, $^{208}Pb/^{207}Pb = 2.448 \pm 0.003$, 2 SD, n = 4) that were within error of previously published results (Table S3). Notably, the repeat GSP analyses yielded Pb isotope data with a long-term precision that was only about a factor of two worse than that obtained for multiple 10 ng filament loads of SRM 981 (Table S3).

3. Results

3.1. Oceanographic regimes

The sampling locations fall within three separate oceanographic

regimes based on temperature and salinity data for surface water samples (Fig. 3, Table 1). The *equatorial zone* (0–20°S) is influenced by the complex pattern of surface currents near the equator, and surface water masses of the northernmost samples are assigned based on salinity to the EUC (35.71; n = 1), the cSEC (36.28; n = 1), and the sSEC (36.85–37.10; n = 3), whilst temperatures are similar (28–29 °C) for all samples in this zone (Sample 66 is excluded as temperature data is not available for it). The *subtropical zone* (20–40°S) of the western South Atlantic is dominated by the Brazil Current. Surface samples collected here show a decrease in both salinity and temperature with latitude, from 36.58 and 26.4 °C at the northernmost station 50, to 35.48 and 20.5 °C at the southernmost station 20, in agreement with observations and modelling studies (Aubone et al., 2021). Lastly, the *subantarctic zone* (40–60°S) is influenced by the confluence of the South Atlantic Current and the Falkland Current at the Brazil-Malvinas Confluence and is separated from the subtropical zone by the Subantarctic Front (Fig. 1). Surface waters collected here show distinctively lower temperatures (21.4 to 10.1 °C) compared to the equatorial zone and lower salinities (34.62 to 33.97) compared to both other zones. Both temperature and salinity decrease southward in the subantarctic zone, in agreement with previous studies (Gordon, 1989).

3.2. Pb concentrations and isotope compositions

The Pb concentrations and isotope compositions of the samples are provided in Table 1 and shown in Figs. 4 and 5. Overall, surface seawater samples (excluding samples 3 and 21b; see SI for explanation) exhibit only limited variability in Pb concentrations and isotope compositions, with a mean Pb concentration of 16.7 ± 3.8 pmol/kg (1 SD, n = 22) and mean Pb isotope compositions of $^{208}Pb/^{207}Pb$ = 2.440 ± 0.007 and $^{206}Pb/^{207}Pb$ = 1.170 ± 0.012 (2 SD, n = 22).

The distribution of surface water Pb concentrations is significantly different between the three zones (ANOVA, p-value < 0.05; Fig. 4). The mean Pb concentrations are highest in the subtropical zone (19.9 ± 2.1 pmol/kg, n = 8, 1SD) and lowest in the subantarctic zone (12.6 ± 2.2 pmol/kg, n = 8, 1SD), with the equatorial zone having an intermediate value of 17.8 ± 1.9 pmol/kg (n = 6, 1SD). The distribution of $^{208}Pb/^{207}Pb$ ratios in surface waters is also significantly different between the three zones (ANOVA, p-value <0.05), whilst the $^{206}Pb/^{207}Pb$ ratios are not statistically distinguishable (ANOVA, p-value >0.05). However, overall, the samples show a limited variability in $^{206}Pb/^{207}Pb$ and $^{208}Pb/^{207}Pb$, with $^{206}Pb/^{207}Pb$ ranging between 1.161 and 1.185, and $^{208}Pb/^{207}Pb$ ranging from 2.433 to 2.446. An additional notable feature is that both $^{206}Pb/^{207}Pb$ and $^{208}Pb/^{207}Pb$ ratios show a higher variability, and larger range, in the subantarctic zone than in the subtropical and equatorial zones (Fig. 4).

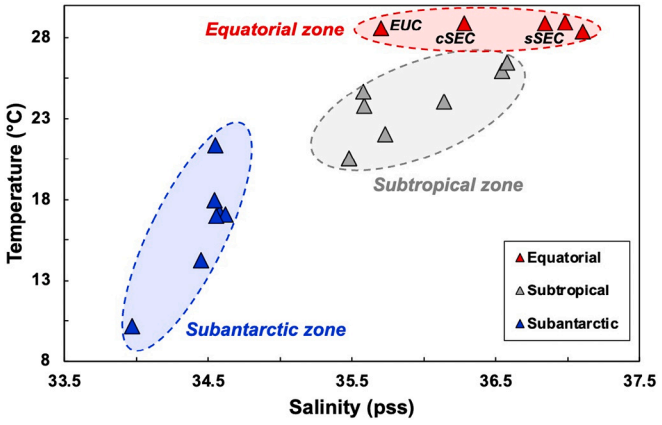

Fig. 3. Temperature and salinity data for the surface water samples analysed in this study, excluding Sample 66 for which temperature data is not available. Triangles represent sample values; ellipses outline the three oceanographic zones. Salinity and temperature data are from Table 1. Abbreviations: EUC – Equatorial Undercurrent; cSEC – central South Equatorial Current; sSEC – southern South Equatorial Current.

3.3. Comparison of Pb concentrations and isotope compositions of filtered and unfiltered seawater samples

No systematic differences are observed between the Pb concentrations determined for two pairs of filtered and unfiltered samples (i.e., dissolved and total dissolvable Pb; samples 4 & 5 and samples 20 & 21a; Table 1). In addition, the total dissolvable Pb concentrations determined here for samples obtained with a Fish from ~3 m water depth can be compared to data from filtered seawater samples collected on the same cruise with the ultra-clean CTD at slightly greater depths (8–10 m) at locations that differ from the Fish samples by up to 0.19° in latitude (Fig. 4; GEOTRACES Intermediate Data Product Group, 2021). The mean total dissolvable Pb concentration of 16.8 ± 4.0 pmol/kg (1 SD, n = 20) is identical within error to the dissolved Pb concentration of 17.0 ± 5.3 pmol/kg (1 SD, n = 16; GEOTRACES Intermediate Data Product Group, 2021; Fig. 4). Expressed in another way, the mean difference between the dissolved and total dissolvable Pb concentrations of the seawater samples is 3.1 ± 17.3 % (1 SD, n = 17). These results suggest that little Pb is held within the >0.2 μm size fraction of surface waters along the cruise track. Therefore, the two filtered (dissolved Pb) samples from this study can be considered equivalent to the unfiltered (total dissolvable Pb) samples.

However, unlike the Pb concentrations, there are small but analytically resolvable differences in the Pb isotope compositions of these two sample pairs (Table 1). In detail, the $^{206}Pb/^{207}Pb$ and $^{208}Pb/^{207}Pb$ ratios for both sample pairs differ outside of error by 200 to 800 ppm (Table 1). The origin of these minor variations is unclear, especially given the essentially identical concentrations of dissolved and total dissolvable Pb. However, small differences in the Pb isotope compositions of particulate and dissolved Pb, or minor effects of contamination during collection, handling, and processing of the samples, could be the reason.

4. Discussion

Lead can be delivered to the surface ocean via atmospheric deposition from regional sources, direct input from local rivers, and atmospheric or oceanic transport from distal source regions. Currently, the vast majority of Pb in the ocean is supplied through atmospheric deposition, which increases the concentration and changes the isotope composition of the dissolved Pb already present in seawater (Patterson and Settle, 1987). Scavenging by particles acts to remove dissolved Pb from seawater but has no significant impact on dissolved Pb isotope compositions (Henderson and Maier-Reimer, 2002). In regions where atmospheric Pb inputs to the surface ocean are low, surface seawaters are therefore expected to have low dissolved Pb concentrations, which may decrease with advection due to scavenging removal, whilst Pb isotope compositions remain essentially unchanged. In the above context, we can think of Pb in a water sample as having two sources: (i) "inherited" Pb, typically Pb from previous atmospheric deposition that is transported by surface currents, and (ii) Pb from recent/regional atmospheric deposition. The balance of these two types of sources will depend on the magnitude and distribution of atmospheric deposition, the residence time of Pb in surface waters, and the pathways and flow speeds of surface currents (Henderson and Maier-Reimer, 2002; Rigaud et al., 2015).

In the following sections, we discuss this balance for each of the three oceanographic zones and provide an analysis of the natural and anthropogenic sources of Pb to the surface waters of the South Atlantic Ocean, both for 2011 and in the context of historical results.

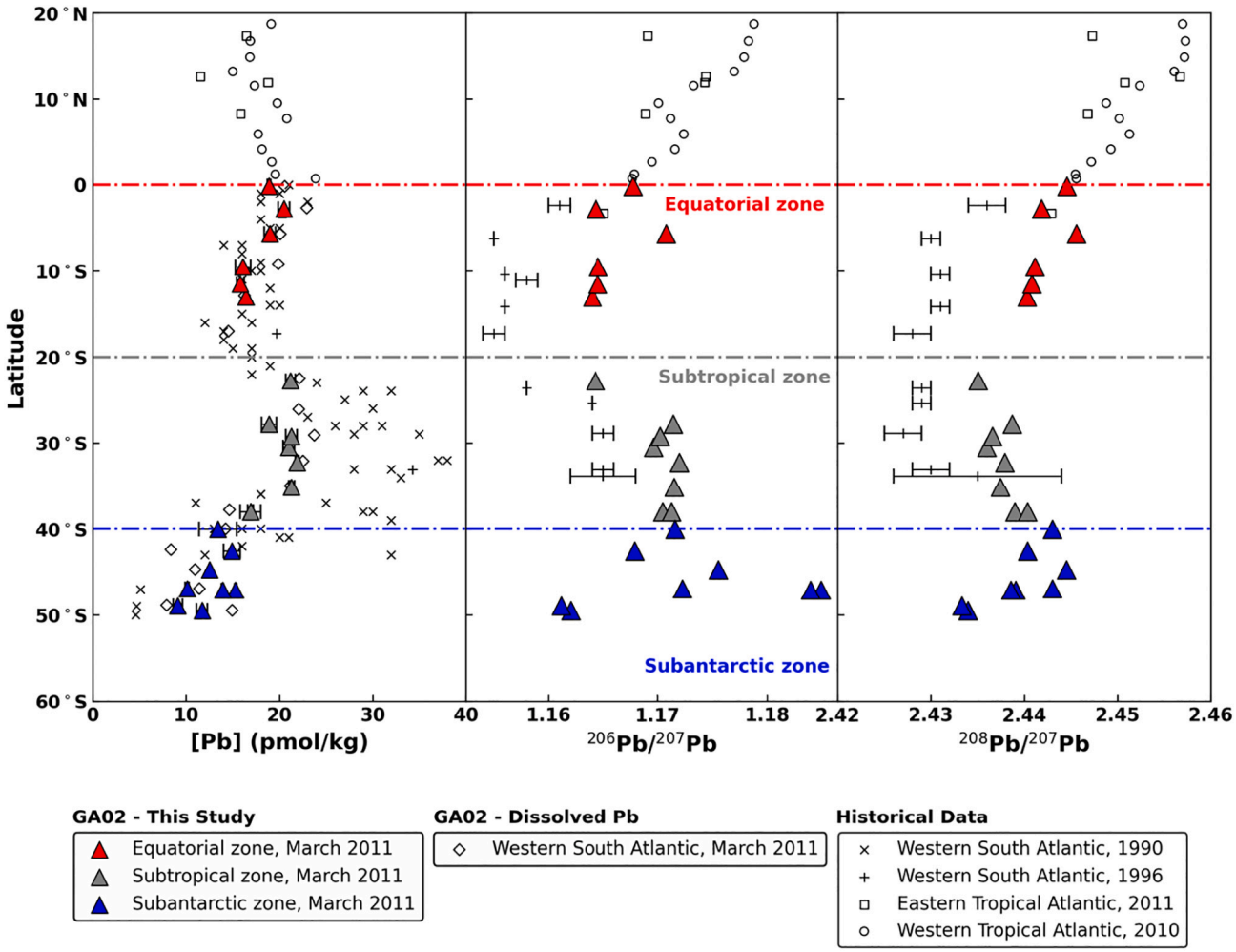

Fig. 4. Latitudinal plots for Pb concentration (left), $^{206}Pb/^{207}Pb$ (centre), and $^{208}Pb/^{207}Pb$ (right). Dashed coloured lines separate the equatorial zone (0–20°S), subtropical zone (20–40°S) and subantarctic zone (40–60°S). Error bars (2SD) for March 2011 isotope data are smaller than symbols, whereas those for concentrations are visible (1SD). Additional dissolved Pb data from GA02: GEOTRACES Intermediate Data Product Group (2021). Historical data: Western South Atlantic 1990 – Helmers and Rutgers van der Loeff (1993); Western South Atlantic 1996 – Alleman et al. (2001a, 2001b); Eastern tropical Atlantic, 2011 – Bridgestock et al. (2016); Western tropical Atlantic, 2010 - Bridgestock et al. (2016). Error bars for Western South Atlantic 1996 isotope data represent 2SD.

4.1. Sources of Pb to the western South Atlantic Ocean

Regional atmospheric sources of Pb include urban and industrial areas of South American countries (predominantly Brazil, Argentina, Uruguay, and Chile), as well as Patagonian dust. The Río de la Plata estuary, formed by the confluence of multiple rivers draining inland areas of Paraguay, Uruguay, Argentina, Brazil, and Bolivia, is the largest source of riverine inputs to the western South Atlantic (Fig. 2), and will be discussed in more detail when assessing Pb sources to the *subtropical zone*. Distal sources of Pb could include urban/industrial areas and deserts of both northern and southern Africa. The signature of such distal inputs can be transported both via atmospheric pathways for approximately 10 days and by ocean currents for a few years, according to the residence times of Pb in the atmosphere and surface ocean, respectively. Transport by surface ocean currents will not only carry the signatures of distal Pb sources but will integrate all Pb sources that were deposited within a time frame shorter than the residence time of Pb in the surface ocean. This scenario is particularly relevant when discussing the signature of "inherited" Pb.

Fig. 2 summarises the potential source areas of Pb for South Atlantic surface waters, based on data currently available. Unfortunately, Pb isotope data for the anthropogenic and natural sources of Angola are not available at present. Such data would be of particular interest because Angola is the second largest oil producer in sub-Saharan Africa and wind patterns indicate that it could be an important source of anthropogenic Pb to the eastern South Atlantic (Fig. 2). Constraints on the isotopic fingerprints of its emissions would therefore help to further unravel the origin of the Pb isotope signatures seen in South Atlantic surface waters. Similarly, Pb isotope data for Brazilian coal are currently not available, so Pb emissions from this source cannot be evaluated as a potential source of Pb to the western South Atlantic Ocean. However, we acknowledge that Brazilian coal production in 2011 was higher than in the 1990s (BP, 2022).

4.1.1. Equatorial zone

Factors that potentially affect the concentration and isotopic composition of Pb in the equatorial zone include atmospheric deposition from distal sources, such as the North African dust plume and North African urban areas, and "inherited" Pb advected from the eastern/south-eastern South Atlantic Ocean via the complex equatorial surface currents. South American sources can be excluded based on the predominant easterly winds at latitudes between 0° and 20°S (Fig. 2), which prevent the transport of atmospheric dust and pollution from the South American continent to the South Atlantic surface ocean in this equatorial region.

Air mass back trajectories generated using the HYSPLIT Trajectory

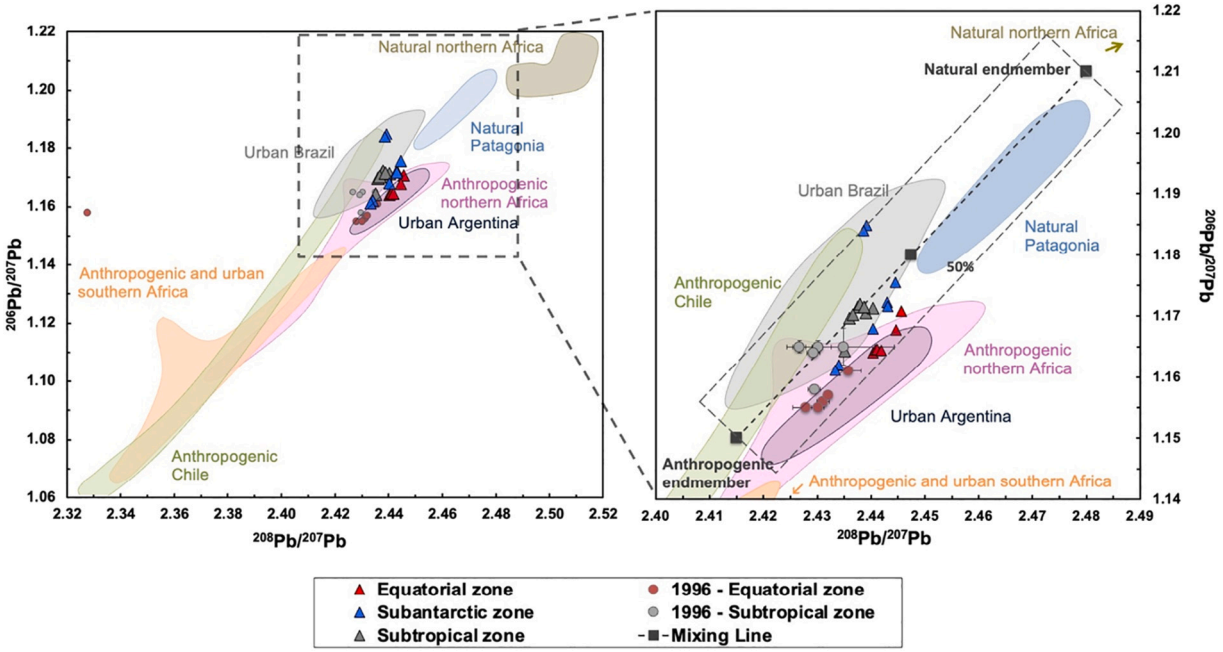

Fig. 5. Three-isotope plots for Pb, showing the compositions of South Atlantic surface seawater samples (symbols) and natural and anthropogenic sources of Pb from Africa and South America (coloured fields). The mixing envelope shows the Pb isotope mixing relationship between the inferred endmembers of anthropogenic Pb ($^{206}Pb/^{207}Pb = 1.150 \pm 0.007$ and $^{208}Pb/^{207}Pb = 2.415 \pm 0.007$) and natural Pb ($^{206}Pb/^{207}Pb = 1.210 \pm 0.007$ and $^{208}Pb/^{207}Pb = 2.480 \pm 0.007$), indicated by the black squares. Error bars (2SD) for the March 2011 isotope data from this study are smaller than the symbols. Error bars for the Western South Atlantic 1996 data represent 2SD.
Data sources: Alleman et al. (2001b), Bollhöfer and Rosman (2000), Khondoker et al. (2018), Gioia et al. (2017), Bridgestock et al. (2016), Kumar et al. (2014) and Witt et al. (2006).

Model (Rolph et al., 2017; Stein et al., 2015) were used to assess the atmospheric pathways for the time and location of the seawater sampling in the equatorial zone in early 2011 (Fig. S1). Back trajectories were computed for seven days for locations placed on an equally spaced matrix in order to cover the entire area. Most trajectories show a particle provenance from the open South Atlantic Ocean to the south-east, and only the far north-western section of the equatorial zone could receive direct atmospheric inputs from the Northern Hemisphere and the Atlantic coast of North Africa due to north-easterly winds near the equator. Only those few trajectories that crossed the equator had paths that encountered land in the seven days prior to sampling, whereas all other trajectories had purely oceanic paths. In addition, wet precipitation within the ITCZ can be expected to remove most of the aerosol load derived from North Africa, hence severely limiting the atmospheric deposition of trace metals derived from North African sources in the equatorial zone (Fig. 2; Adams et al., 2012; Schlosser et al., 2014). Further support for this conclusion is provided by the low annual average dust deposition flux estimates (Kok et al., 2021), which are lower than 1 g m^{-2} yr^{-1} for most of the equatorial zone, with values up to 5 g m^{-2} yr^{-1} only between 0° and 5°S. Therefore, the distribution of Pb isotopes in the surface waters of the equatorial western South Atlantic must be driven by a different mechanism.

Based on the hydrography of the region, surface currents can be regarded as a source of "inherited" Pb to the equatorial zone (Fig. 1). The northern part of the South Atlantic basin has numerous surface currents and undercurrents that interact with each other and with their northern equatorial counterparts, whilst maintaining their distinct oceanographic characteristics (e.g., salinity). Notably, the Pb isotope composition and salinity of the equatorial samples are compatible with the distribution of the currents, and therefore surface oceanography seems key to the interpretation of Pb isotope compositions observed in this zone.

Samples 52, 53, and 54 (9.5 to 13.0°S) coincide with the sSEC (Fig. 3) and have a nearly uniform isotopic signature of $^{208}Pb/^{207}Pb = 2.441 \pm 0.001$ and $^{206}Pb/^{207}Pb = 1.164 \pm 0.001$ (2 SD, n = 3), suggesting that the sSEC has a well-mixed Pb isotope composition. These Pb isotope compositions closely resemble the composition of surface waters in the eastern South Atlantic Ocean, which are influenced by aeolian inputs from South America (Paul et al., 2015b), thereby supporting this "inherited" origin. In addition, such agreement indicates that these samples were not influenced or were only marginally influenced by Northern Hemisphere emissions.

Sample 65 (5.7°S, 28.5°W) coincides with the cSEC (Fig. 3) and is characterised by $^{208}Pb/^{207}Pb = 2.446$ and $^{206}Pb/^{207}Pb = 1.171$. Although the cSEC and sSEC both originate in the equatorial eastern Atlantic, and presumably receive similar atmospheric inputs, they appear to differ in their Pb isotope signature. Sample 65 has the highest $^{208}Pb/^{207}Pb$ and $^{206}Pb/^{207}Pb$ ratios of samples from the equatorial zone and agrees with the Pb isotope composition of seawater samples collected north of the equator in the eastern and western tropical Atlantic (Bridgestock et al., 2016). Most likely, these observations reflect an input of Pb sourced from the Northern Hemisphere through mixing in the Angola Gyre, which is partially fed by surface and subsurface currents that originate north of the equator (i.e., EUC and Gabon-Congo Undercurrent; Stramma and Schott, 1999), and which itself feeds into the cSEC.

Sample 67 (0.2°S, 32.9°W) coincides with the expected location of the EUC, and was collected during Northern Hemisphere spring, when the EUC is located at shallower depths. Its salinity matches well with other literature values for the salinity of this current, suggesting that Sample 67 is indeed from the EUC (Fig. 3; Table 1; Da-Allada et al., 2017; Metcalf et al., 1962). Its Pb isotope composition ($^{208}Pb/^{207}Pb = 2.445$ and $^{206}Pb/^{207}Pb = 1.168$) is intermediate between the compositions of samples 52–54 and Sample 65, in accord with previous work suggesting that the EUC is formed from the sSEC and cSEC (via the NBC; Stramma and Schott, 1999).

Sample 66 (2.8°S, 28.9°W) is located between the EUC and the cSEC. Surprisingly, its Pb isotope composition is distinct from both neighbouring currents, but very similar to the sSEC samples. Bridgestock et al.

(2016) reported a comparable result of $^{208}Pb/^{207}Pb$ = 2.4429 and $^{206}Pb/^{207}Pb$ = 1.1651 for a sample collected 20 days before Sample 66 (on 05/03/2011) at 3.31°S, 25.49°W, as part of the GEOTRACES section GA06. The GA06 sampling location has a salinity that is intermediate between those of samples 67 and 65, and higher compared to Sample 66 (Table 1). However, since no temperature data is available for Sample 66, only a speculative explanation can be provided. One possibility is that the two locations were on the trajectory of an equatorial eddy or a tropical instability wave travelling westward (Aguedjou et al., 2019; Chelton et al., 2011; de Decco et al., 2018), which could carry an atypical Pb isotope composition to this location. Indeed, Paul et al. (2015b) previously showed that the Pb isotope signal of mesoscale eddies is trackable in the South Atlantic Ocean.

Overall, the Pb distribution in the equatorial zone appears to be controlled mostly by surface currents, which transport Pb that was previously deposited both in the South Atlantic and in the equatorial region of the North Atlantic, rather than by direct atmospheric deposition, and thus primarily shows an "inherited" signature. This interpretation is supported by the timescale of surface current movement for the SEC, as its flow speed varies between 10 and 30 cm s^{-1} (Peterson and Stramma, 1991). As such, it takes between 4 and 12 months for a water parcel to travel from east to west in the equatorial South Atlantic, which is less than the residence time of Pb in surface waters (2–3 years; Bacon et al., 1976; Kadko et al., 2020; Nozaki et al., 1976).

4.1.2. Subtropical zone

Samples from the subtropical zone were collected at latitudes coinciding with the highly populated and urbanised coastal cities of Brazil (i.e., Rio de Janeiro, São Paulo, Belo Horizonte, Porto Alegre), as well as Buenos Aires and Montevideo. The latter cities are located on the shores of the Río de la Plata estuary (Fig. 2), which very likely acquires an urban Pb isotope signature from surface run-off as well as industrial and municipal waste discharges. Most Pb is effectively scavenged by particles in estuaries, reducing the flux of dissolved riverine Pb to the oceans (Cindrić et al., 2015; Dai and Martin, 1995; Marsan et al., 2014). On the other hand, isotope exchange between dissolved and particulate Pb at the land-ocean boundary has been recently shown to occur without considerable effects on Pb concentrations (Chen et al., 2023). Considering the large distance of approximately 1000 km between the coast and all sampling locations (Fig. 1), the lack of evidence for changes in salinity along the cruise transect (Table 1), and the effective scavenging of Pb in estuaries, it is unlikely that the Río de la Plata is a significant direct source of Pb to the surface waters of the subtropical zone.

Having ruled out a major control by fluvial Pb sources, we therefore focus on potential atmospheric Pb sources to the subtropical zone. South American sources with known Pb isotope compositions include urban dust and aerosols from São Paulo and Buenos Aires (Aily, 2001; Babinski et al., 2003; Bollhöfer and Rosman, 2000; Gioia et al., 2010, 2017; Khondoker et al., 2018; Souto-Oliveira et al., 2018), which reflect mainly industrial activities and urban traffic (i.e. fuels, road dust, including brake and tyre wear and road surface abrasion), as well as Patagonian dust (Khondoker et al., 2018). There is a substantial range in Pb isotope compositions of aerosols and dust from São Paulo (e.g. $^{208}Pb/^{207}Pb$ = 2.355–2.464 and $^{206}Pb/^{207}Pb$ = 1.149–1.328, Gioia et al., 2017; $^{208}Pb/^{207}Pb$ = 2.412–2.482 and $^{206}Pb/^{207}Pb$ = 1.143–1.272, Aily, 2001). However, here we choose to use the signature of the main sources of Pb, specifically aerosols and road dust, that capture the main contributions of traffic pollution from 'urban Brazil' (Bollhöfer and Rosman, 2000; Gioia et al., 2017; Khondoker et al., 2018; Fig. 5).

All sampling stations within the subtropical zone are located in an area of high precipitation in the central western South Atlantic related to the SACZ (Fig. 2). In such a setting, we expect that any atmospheric Pb that is carried east or south-east from these urban areas to the western South Atlantic will be efficiently washed out by precipitation, thereby entering the surface ocean through wet deposition. Indeed, all samples collected in the subtropical zone have Pb isotope compositions that are consistent with sources from 'urban Brazil' (Fig. 5). In addition, the mean Pb concentration of samples from the subtropical zone (19.9 ± 2.1 pmol/kg, n = 8, 1SD) is 24 % higher than the Pb concentration of the southernmost samples from the equatorial zone (16.1 ± 0.3 pmol/kg, n = 3, 1SD; Fig. 4). The latter samples were collected in the sSEC, which feeds into the Brazil Current, from which the subtropical zone samples were collected, so this increase in Pb concentrations also attests to the addition of Pb inputs from land.

Air mass back trajectories generated using the HYSPLIT Trajectory Model for the subtropical zone show variable oceanic paths, reflecting the complex atmospheric circulation in the South Atlantic basin (Fig. S2). The northern section of the subtropical zone appears to be mainly subject to atmospheric transport that follows purely oceanic pathways from the east, with a similar pattern to that observed for most of the equatorial zone. However, some more northerly or westerly air mass trajectories originate over inland Brazil, which indicates that atmospheric transport from land is a possible source. In fact, although the general atmospheric circulation patterns suggest that winds blow mainly onshore in the industrialised areas of Rio de Janeiro, São Paulo, Belo Horizonte, Porto Alegre, Montevideo, and Buenos Aires (Fig. 2), westerly wind anomalies are observed in this region during austral summer months in relation to the SACZ and the South American Monsoon System (SAMS; Carvalho et al., 2004; Jones and Carvalho, 2002). Meanwhile, the southernmost latitudes of the subtropical zone have back trajectories that pass over the southern tip of South America, extending back to the Pacific Ocean and in some cases as far as Antarctica. Therefore, it is also possible that dust from Patagonia could reach these surface waters and mix with the signature of urban South American sources. However, based on the Pb isotope composition of the samples, Patagonian dust cannot be the predominant source of Pb to the subtropical surface waters (Fig. 5).

The Pb isotope compositions of the surface water samples in the subtropical zone match well with anthropogenic inputs from the Sao Paulo metropolitan area (i.e., 'urban Brazil' in Fig. 5), which is on the trajectory identified by wind patterns and HYSPLIT simulations (Fig. S2). These findings support that the direct deposition of atmospheric Pb transported from land is the predominant source of Pb to the subtropical zone of the western South Atlantic Ocean. Since the Pb isotope compositions of samples from Buenos Aires are not very different from those of Sao Paulo, and since the wind patterns also do not exclude it, Buenos Aires cannot be ruled out as an additional source. The predominance of direct atmospheric anthropogenic inputs over an "inherited" Pb signal is also supported by the higher Pb concentrations of surface waters in the subtropical zone compared to the equatorial and subantarctic zones. This conclusion is also in accord with the fairly uniform Pb isotope composition observed for the surface seawater of the subtropical zone ($^{208}Pb/^{207}Pb$ = 2.438 ± 0.003 and $^{206}Pb/^{207}Pb$ = 1.170 ± 0.005, 2 SD, n = 8), which is compatible with 'urban Brazil' sources, whereas a predominance of "inherited" Pb from the Brazil Current would result in a Pb isotope composition more similar to that of the equatorial zone (Fig. 5).

Overall, the similar Pb isotope compositions of seawater samples and anthropogenic/urban sources of South America, as well as wind patterns, air mass back trajectories, and the elevated Pb concentrations, indicate that South American urban and industrial emissions are the dominant source of Pb to the surface ocean of the subtropical zone.

4.1.3. Subantarctic zone

The subantarctic zone at 40–60°S is located between the Subtropical and Subantarctic Fronts and is subject to strong westerly winds. Here, the most prominent potential sources of Pb include urban and industrial emissions from South America, as well as mineral dust from Patagonia (Fig. 2). Of the three zones analysed, the subantarctic zone has the highest dust deposition fluxes of up to 10 g m^{-2} yr^{-1}, which suggests that mineral dust signatures might be more discernible in surface water

samples from this region (Kok et al., 2021). Based on our data, surface seawater of the subantarctic zone has the lowest mean Pb concentration (12.6 ± 2.2 pmol/kg, n = 8, 1 SD) and the most variable Pb isotope composition of the three zones, with $^{208}Pb/^{207}Pb$ varying between 2.433 and 2.445, and $^{206}Pb/^{207}Pb$ between 1.161 and 1.185 (Figs. 4, 5). This variability in Pb isotope composition combined with low Pb concentrations, which would make the isotopic signature of seawater more susceptible to local Pb additions with differing isotopic compositions, suggests that mixing of Pb from different sources and the removal of Pb by scavenging could both play an important role in this region (Fig. 5).

All samples collected in the subantarctic zone have Pb isotope compositions that overlap with South American urban sources, either coinciding with the 'urban Brazil' signature, or potentially reflecting a mixture of 'urban Brazil', 'urban Argentina', and 'natural Patagonia' sources (Fig. 5). Samples 4 and 5, which were collected at the same location for dissolved and total dissolvable Pb samples (and are therefore considered to be the same), show isotope compositions that differ from those of the other subantarctic zone samples (i.e. elevated $^{206}Pb/^{207}Pb$ ratios), making those the only samples well within the 'urban Brazil' field (Fig. 5). In particular, they differ significatively from Sample 16, which was collected using the ultra-clean CTD approximately 17 km to the east and only 5 h later. Temperature and salinity data do not suggest the presence of different water masses between Samples 4 and 5 and Sample 16 (Table 1; Fig. S3). Furthermore, Cd, Fe, and Mn concentrations show good agreement between the locations (GEOTRACES Intermediate Data Product Group, 2021; Middag et al., 2015; van Hulten et al., 2017; Xie et al., 2015). However, Sample 5 shows a significantly elevated Al concentration of 5.2 nmol/kg (Fig. S4). It is important to note here that samples collected for different elements were stored in different sample bottles and sampled at slightly different times. Therefore, we suggest that the similar Pb, Cd, and Fe concentrations of samples 4, 5, and 16 argue against contamination as a source for the different Pb isotope signatures, and instead we suggest a different environmental source for Samples 4 and 5.

The dominant winds in the subantarctic zone are westerlies (Fig. 2), but air mass back trajectories generated with the HYSPLIT Trajectory Model for the subantarctic zone show some variability. Particle trajectories crossed land at different latitudes, but predominantly over the southern region of South America, coinciding with Patagonia (Fig. S5). In the seven days before deposition, some particles traversed Southern Argentina, where several oil production sites are located (Curia et al., 2018), before traversing parts of the South Pacific and Southern Ocean. Given this range of pathways, a wide range of atmospheric sources should be considered, including anthropogenic emissions from South America and natural dust from Patagonia. In addition to the trajectory simulations, the general atmospheric circulation patterns (Fig. 2) also support the proposal that both mineral dust from Patagonia and anthropogenic Pb from South American sources could have influenced Pb isotopes in the subantarctic zone of the western South Atlantic Ocean (Fig. 5).

The vast majority (95 %) of mineral dust generated in South America is from Patagonia (Johnson et al., 2010), which in turn is predominantly deposited in the southern section of the South Atlantic Ocean between 30 and 60°S (Jickells et al., 2005; Kok et al., 2021). Dust production varies seasonally and can occur in discrete events (Gaiero et al., 2003; Gassó and Stein, 2007). In terms of Pb isotopes, Patagonian dust has high $^{208}Pb/^{207}Pb$ and $^{206}Pb/^{207}Pb$ ratios of 2.469 ± 0.013 and 1.195 ± 0.013, respectively (2 SD, n = 29; Khondoker et al., 2018; Fig. 5). These values are higher than those determined for any of our seawater samples, which points to mixing between South American anthropogenic Pb from Southern Argentina, where several oil fields are located, and natural Patagonian Pb from higher latitudes. However, the lack of published data on the Pb isotope composition of Argentinian oil field sources only allows for a speculative interpretation at present, and future studies are needed to confirm this.

Lead concentrations are lower in the surface waters of the subantarctic zone than in the subtropical zone (Fig. 4). As dissolution rates of natural atmospheric particles are up to 100 times slower than those of anthropogenic-sourced Pb (Bridgestock et al., 2016; Hsu et al., 2005), the reduced anthropogenic contribution to atmospheric particles in this region could help to explain the lower surface water Pb concentrations in the subantarctic zone. Moreover, Pb solubility decreases with increasing dust loads (Benaltabet et al., 2020; Guerzoni et al., 1999; Hsu et al., 2005). In addition, higher terrigenous particle loads, as well as higher rates of biogenic particle production in the subantarctic zone, as reflected in higher fluorescence values (Xie et al., 2015), are likely to contribute to higher scavenging rates for Pb in the surface ocean (Cochran et al., 1990). The high rates of biogenic particle production in the subantarctic zone are caused by mixing at the Subtropical Front (40°S, Fig. 1) between oligotrophic, warm (>20 °C), and saline (>34.5) surface waters of the central South Atlantic and the cooler (<11 °C), fresher (<34.0), nutrient-rich surface waters of the Antarctic Circumpolar Current (Table 1).The strong scavenging activity is also supported by the agreement between lower Pb concentrations and lower Al concentrations in surface waters in this region (Middag et al., 2015).

In summary, the Pb concentrations and isotope compositions, air mass back trajectories, and dust deposition fluxes support the conclusion that Pb is supplied to the subantarctic zone by direct atmospheric deposition, from both anthropogenic emissions and natural Patagonian dust sources. The lower Pb concentrations observed in the subantarctic zone can be explained by the lower solubility of naturally sourced Pb compared to anthropogenic Pb and by the stronger scavenging of Pb in this region.

4.2. *Anthropogenic and natural Pb in the South Atlantic Ocean: temporal changes and mass balance*

Lead concentrations and isotope compositions in the South Atlantic Ocean can be attributed to different predominant sources of Pb, which vary spatially according to the different oceanographic and atmospheric regimes. When compared to literature data, our new results can also be used to investigate the temporal evolution of the Pb isotope signature in the surface waters of the western South Atlantic, and hence changes in those source contributions through time.

4.2.1. *Decline in surface water Pb concentrations from 1990 to 2011*

Analyses of seawater samples collected at similar latitudes and longitudes in the 1990s show a similar pattern of Pb concentrations to those presented here, with Pb concentrations highest in the subtropical zone, followed by the equatorial zone, and lowest in the subantarctic zone (Helmers and Rutgers van der Loeff, 1993; Alleman et al., 2001a; Fig. 4). In all three zones, mean Pb concentrations in March 2011 were lower than or equal to those of 1990 and 1996. In detail, Pb concentrations in the surface waters of the equatorial zone in November 1990 (17.8 ± 2.8 pmol/kg, 1 SD, n = 28; Alleman et al., 2001a; Helmers and Rutgers van der Loeff, 1993) were essentially identical to those observed in March 2011 in this study (17.8 ± 1.9 pmol/kg, 1 SD, n = 6; Fig. 6). The more variable Pb concentrations of the subantarctic zone in November 1990 define a mean (14.8 ± 8.3 pmol/kg, 1 SD, n = 11; Helmers and Rutgers van der Loeff, 1993) that is slightly elevated compared to the mean observed in March 2011 (12.6 ± 2.2 pmol/kg; 1 SD, n = 8; Fig. 6). However, due to the large variability in Pb concentrations in the 1990 dataset, both values are statistically identical ($p > 0.05$, *t*-test). The largest deviations between historical and more recent Pb concentrations are observed for the subtropical zone (Fig. 6). In detail, the Pb concentrations from November 1990 define a distinctly elevated mean (32.7 ± 18.4 pmol/kg, 1 SD, n = 32; Helmers and Rutgers van der Loeff, 1993 Alleman et al., 2001a) compared to the March 2011 data (19.9 ± 2.1 pmol/kg, 1 SD, n = 8), although both datasets are again statistically identical ($p > 0.05$, *t*-test) due to the highly variable historical Pb concentrations.

When combining the historical data of all three zones, they define a

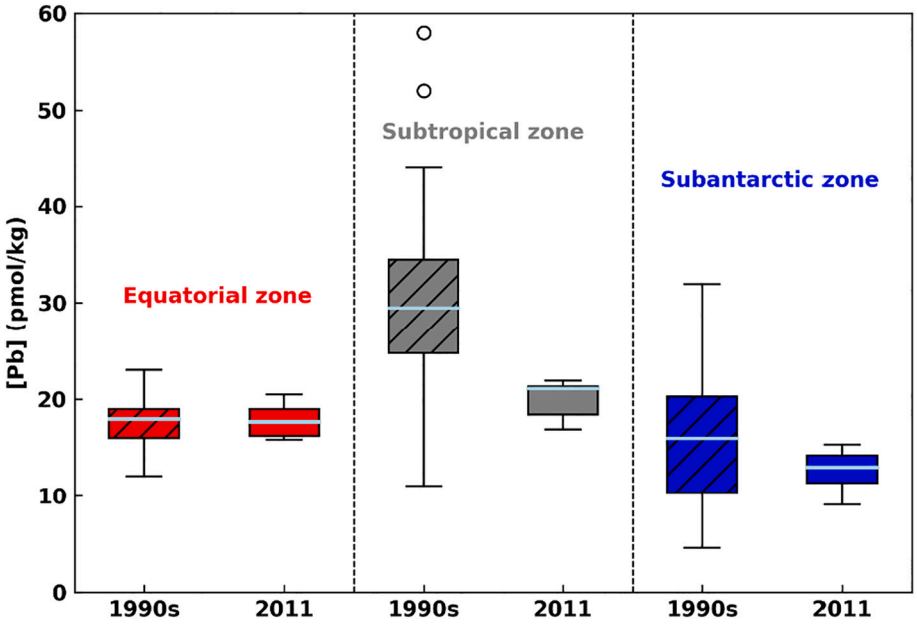

Fig. 6. Average Pb concentrations of surface water from the equatorial, subtropical, and subantarctic zones of the western South Atlantic in the 1990s (Helmers and Rutgers van der Loeff, 1993; Alleman et al., 2001b) and 2011 (this study). For each dataset, the light blue lines represent the median, shaded boxes extend from the first quartile to the third quartile, whilst whiskers extend from the box by 1.5× the interquartile range, encompassing all data points that are not 'outliers'; open circles are 'outliers'. (For interpretation of the references to colour in this figure legend, the reader is referred to the web version of this article.)

mean Pb concentration for the surface western South Atlantic Ocean that was 34 % lower in March 2011 (16.7 ± 3.8 pmol/kg, 1 SD, n = 22) than in the 1990s (25.2 ± 18.1 pmol/kg, 1 SD, n = 71; Helmers and Rutgers van der Loeff, 1993; Alleman et al., 2001a). Notably, the historical and March 2011 means are statistically different ($p < 0.05$, *t*-test) when the larger datasets, which are obtained by combining data from all three zones, are compared. However, the observed change is predominantly driven by the temporal decrease in the Pb concentrations of the subtropical zone, which is most strongly impacted by South American anthropogenic and urban inputs. This finding supports the hypothesis that national policies of South American countries to ban the use of tetraethyl lead in gasoline led to a decrease in anthropogenic Pb inputs from South America. Brazil completely phased out leaded petrol in 1991 (Eichler et al., 2015) and Argentina did so by 1996 (Lovei, 1996), whilst Uruguay and Chile continued using leaded petrol until 2004 and 2005, respectively (Mañay et al., 2008; Queirolo et al., 2010; Eichler et al., 2015). Compared to the 34 % decrease in the mean Pb concentration of surface waters of the western South Atlantic Ocean between 1990 and 2011, the western North Atlantic experienced an 80 % decrease in the mean Pb concentration of surface waters between 1970 and 2000, as inferred from seawater data (Boyle et al., 2014) and coral records off Bermuda (Kelly et al., 2009), mainly due to the greater historical anthropogenic Pb loading in that region, and possibly due to the longer timescale of comparison.

4.2.2. *Shift in surface water Pb isotope compositions from 1990 to 2011*

The Pb isotope data available for the South Atlantic surface waters, together with the potential natural and anthropogenic sources, can be used to interrogate whether the inferred 34 % decline in South Atlantic surface water mean Pb concentrations is consistent with lower emissions of anthropogenic Pb and the phasing out of leaded gasoline. For this purpose, we use a simple isotope mass balance model (Table S6) since most natural and anthropogenic South American Pb sources have isotope compositions that can be used to define two distinct endmembers (Fig. 5): (i) an anthropogenic endmember with $^{206}Pb/^{207}Pb = 1.150 \pm 0.007$ and $^{208}Pb/^{207}Pb = 2.415 \pm 0.007$, which approximates the Pb isotope signature of urban and industrial eastern South American sources as defined by a mixture of the lowest $^{206}Pb/^{207}Pb$ and $^{208}Pb/^{207}Pb$ ratios observed for Buenos Aires and 'urban Brazil'; and (ii) a natural endmember with $^{206}Pb/^{207}Pb = 1.210 \pm 0.007$ and $^{208}Pb/^{207}Pb = 2.480 \pm 0.007$, which represents the average Pb isotope signature of Patagonian and North African mineral dust. The quoted uncertainties on those endmember values account for both variability in the compositions of the anthropogenic and natural Pb sources and changes in source relevance with latitude (i.e., North Africa is most relevant for the equatorial zone due to water mixing between surface currents north and south of the equator, Brazil for the subtropical zone, and Argentina for the subantarctic zone). To calculate the percentage of natural and anthropogenic Pb in each sample, the data points in the $^{206}Pb/^{207}Pb$ vs $^{208}Pb/^{207}Pb$ space which did not plot exactly on the mixing line ($y = 0.923x - 1.079$, where y is $^{206}Pb/^{207}Pb$ and x is $^{208}Pb/^{207}Pb$) were projected onto it.

Based on the inferred endmember compositions, the Pb isotope compositions of the South Atlantic surface waters collected in 2011 indicate that 25–47 % of the Pb present in the samples is of a natural origin across the South Atlantic, with a mean contribution of 36 ± 6 % (1 SD, n = 22; Fig. 5, Table S6). This estimate demonstrates that the Pb inventory of surface waters in the western South Atlantic Ocean is still dominated by anthropogenic sources, but that the natural Pb signal is stronger than it was in 1996. Indeed, using the same calculation, natural Pb accounted for only 24 ± 4 % of the Pb found in surface seawater from the equatorial and subtropical western South Atlantic in 1996 (1 SD, n = 11; Fig. 5; Alleman et al., 2001b). This temporal shift towards a more natural Pb isotope signature is statistically significant ($p < 0.05$, *t*-test), and is in accord with the decrease in leaded gasoline emissions, as countries bordering the South Atlantic Ocean phased out its use. The increase in the relative abundance of natural Pb between the 1990s and 2011 is also observed when including the two previously defined endmembers in a concentration mass balance calculation, which shows that natural Pb accounts for 38 % and anthropogenic Pb for 62 % of the total Pb concentration in 2011, in line with the results obtained from the isotopic mass balance (see note in SI).

Our estimate for the contributions of natural versus anthropogenic Pb to South Atlantic surface waters is similar to a recent estimate for the low-latitude North Atlantic Ocean. In detail, Bridgestock et al. (2016) found that natural Pb accounts for 30–50 % of the total Pb present in tropical North Atlantic surface waters. The similar range in relative abundance of natural Pb appears to be a surprising result, since historical Pb concentrations were less elevated by anthropogenic emissions in South Atlantic surface waters (peak values of 118 pmol/kg in 1990; Helmers and Rutgers van der Loeff, 1993) than in the North Atlantic Ocean (peak values of ~250 pmol/kg in 1970; Kelly et al., 2009). This

difference reflects the much larger historical emissions of Pb from American and European pollution sources in the Northern Hemisphere, compared to those from countries bordering the South Atlantic Ocean (Pacyna and Pacyna, 2001). However, the North Atlantic also receives an input of 194 Tg yr^{-1} of mineral dust from Africa, whilst the South Atlantic receives <10 % of this mass flux from South America (Jickells et al., 2005). As a result, mixing calculations to determine the relative proportions of natural versus anthropogenic Pb inputs to both regions yield similar changes over time. As for the North Atlantic Ocean, the South Atlantic has seen a return of natural Pb to surface waters since the 1990s, providing evidence for the success of environmental policies that have progressively banned the use of leaded gasoline over the past 50 years. Nevertheless, even though leaded gasoline has now been banned worldwide, more than half of the Pb in the surface waters of the western South Atlantic Ocean is still of anthropogenic origin, indicating that efforts are still required to minimise other sources of anthropogenic Pb pollution, such as coal combustion. Additionally, we suspect that Pb from past emissions could be recycled and remobilised in terrestrial environments and contribute to anthropogenic Pb inputs to surface water via atmospheric deposition of dust and aerosols. Future studies are needed to confirm the significance of such a source of anthropogenic Pb to the surface ocean.

5. Conclusions

Lead concentration and isotope composition data are presented for 23 surface seawater samples collected in March 2011 during Leg 3 of the GEOTRACES GA02 cruise. Based on regional surface hydrography, the western South Atlantic Ocean was divided into three different oceanographic regimes and the sources of Pb to each zone were identified. The equatorial zone, extending between 0 and 20°S, was characterised by a strong signal of "inherited" marine Pb advected by the surface and subsurface equatorial currents, with a limited Northern Hemisphere signal from atmospheric aerosols at latitudes close to the equator. The main source of Pb to the subtropical zone, between 20° and 40°S, was urban pollution from South American cities such as Sao Paulo. Finally, the subantarctic zone, between 40° and 60°S, had the most variable Pb isotope compositions, suggesting a mixed origin of Pb, including both anthropogenic sources from South America and natural dust sources from Patagonia.

Mean Pb concentrations in the surface waters of the western South Atlantic Ocean decreased by 34 % between the 1990s and 2011, in line with a shift in Pb isotopes towards compositions that are less dominated by urban and industrial Pb sources. In detail, the Pb isotope compositions of samples collected in 2011 suggests that, on average, natural Pb sources contributed 36 ± 6 % of the Pb present in western South Atlantic surface waters, compared to 24 ± 4 % in 1996. This shift towards a more natural Pb isotope signal provides evidence for the positive effect of environmental and health policies that banned the use of leaded gasoline in South America since the 1990s. However, it is notable that anthropogenic Pb still dominates the budget of total dissolvable Pb in western South Atlantic surface waters, which indicates that other sources of pollution need to be minimised to further restore the natural biogeochemical cycle of Pb in the ocean.

Funding

Arianna Olivelli was supported by the Natural Environment Research Council (NE/S007415/1). Katy Murphy was supported by the Natural Environment Research Council (NE/J021636/1). Dominik Weiss, Tina van de Flierdt, and Mark Rehkämper were supported by the Natural Environment Research Council (NE/H006095/1). David Wilson was supported by the Leverhulme Trust (RPG-398) and a Natural Environment Research Council independent research fellowship (NE/T011440/1). The GEOTRACES GA02 section cruises were financed by the Netherlands Organization for Scientific Research (NWO) project grant 839.08.410. For the purpose of open access, the author has applied a Creative Commons Attribution (CC BY) license to any Author Accepted Manuscript version arising.

CRediT authorship contribution statement

Mark Rehkämper (MR), Tina van de Flierdt (TvdF), and Dominik Weiss (DW) devised the project. DW collected the samples supported by numerous colleagues and crew on the third leg of the Dutch GA02 GEOTRACES section, including Micha Rijkenberg and Rob Middag. Katy Murphy carried out all lab work, supported by Luke Bridgestock and David Wilson, and wrote an initial version of the text in the form of a PhD thesis chapter, with support and guidance from TvdF and MR. Arianna Olivelli produced all tables and figures, developed the final data interpretation, and wrote the final manuscript, with input from all co-authors.

Declaration of competing interest

The authors declare that they have no known competing financial interests or personal relationships that could have appeared to influence the work reported in this paper.

Data availability

The data will be available via GEOTRACES.

Acknowledgements

Barry Coles and Katharina Kreissig are thanked for keeping the TIMS and clean room laboratories running smoothly. Eric Achterberg is thanked for providing unpublished salinity and temperature data for GEOTRACES GA06. We also thank two anonymous reviewers for their constructive comments on an earlier version of the manuscript.

Appendix A. Supplementary data

Supplementary data to this article can be found online at https://doi.org/10.1016/j.marpolbul.2023.114798.

References

Adams, A.M., Prospero, J.M., Zhang, C., 2012. CALIPSO-derived three-dimensional structure of aerosol over the Atlantic basin and adjacent continents. J. Clim. 25 (19), 6862–6879. https://doi.org/10.1175/JCLI-D-11-00672.1.

Aguedjou, H.M.A., Dadou, I., Chaigneau, A., Morel, Y., Alory, G., 2019. Eddies in the tropical Atlantic Ocean and their seasonal variability. Geophys. Res. Lett. 46 (21), 12156–12164. https://doi.org/10.1029/2019GL083925.

Aily, C., 2001. Caraterização Isotópica de Pb na Atmosfera: um Exemplo da Cidade de São Paulo. Univesidade de São Paulo.

Alleman, L.Y., Church, T.M., Ganguli, P., Hamelin, B., Flegal, A.R., 2001a. Role of oceanic circulation on contaminant lead distribution in the South Atlantic. Deep-Sea Res.II 48, 2855–2876.

Alleman, L.Y., Church, T.M., Véron, A.J., Kim, G., Hamelin, B., Flegal, A.R., 2001b. Isotopic evidence of contaminant lead in the South Atlantic troposphere and surface waters. Deep-Sea Res.Part II: Top.Stud.Oceanogr. 48 (13), 2811–2827. https://doi.org/10.1016/S0967-0645(01)00019-4.

Aubone, N., Palma, E.D., Piola, A.R., 2021. The surface salinity maximum of the South Atlantic. Prog. Oceanogr. 191 https://doi.org/10.1016/j.pocean.2020.102499.

Babinski, B.M., Aily, C., Ruiz, I.R., Sato, K., 2003. Pb isotopic signatures of the atmosphere of the São Paulo city. J. Phys. IV France 107, 87–90.

Bacon, M.P., Spencer, D.W., Brewer, P.G., 1976. 210Pb/226Ra and 210Po/210Pb disequilibria in seawater and suspended particulate matter. Earth Planet. Sci. Lett. 32, 277–296.

Benaltabet, T., Lapid, G., Torfstein, A., 2020. Seawater Pb concentration and isotopic composition response to daily time scale dust storms in the Gulf of Aqaba,Red Sea. Mar. Chem. 227, 103895 https://doi.org/10.1016/j.marchem.2020.103895.

Bollhöfer, A., Rosman, K.J.R., 2000. Isotopic source signatures for atmospheric lead: the Southern Hemisphere. Geochim. Cosmochim. Acta 64 (19), 3251–3262.

Bombardi, R.J., Carvalho, L.M.V., Jones, C., Reboita, M.S., 2014. Precipitation over eastern South America and the South Atlantic Sea surface temperature during neutral ENSO periods. Clim. Dyn. 42 (5–6), 1553–1568. https://doi.org/10.1007/s00382-013-1832-7.

Bourlès, B., Gouriou, Y., Chuchla, R., 1999. On the circulation in the upper layer of the western equatorial Atlantic. J. Geophys. Res. Oceans 104 (C9), 21151–21170. https://doi.org/10.1029/1999jc900058.
Boyle, E.A., Lee, J.M., Noble, A.E., Moos, S., Carrasco, G., Zhao, N., Kayser, R., Zhang, J., Gamo, T., Obata, H., Norisuye, K., 2014. Anthropogenic lead emissions in the ocean: the evolving global experiment. Oceanography 27 (1), 69–75. https://doi.org/10.5670/oceanog.2011.80.
BP, 2022. Statistical Review of World Energy 2022.
Brandt, P., Schott, F.A., Provost, C., Kartavtseff, A., Hormann, V., Bourlès, B., Fischer, J., 2006. Circulation in the central equatorial Atlantic: mean and intraseasonal to seasonal variability. Geophys. Res. Lett. 33 (7) https://doi.org/10.1029/2005GL025498.
Bridgestock, L., van de Flierdt, T., Rehkämper, M., Paul, M., Middag, R., Milne, A., Lohan, M.C., Baker, A.R., Chance, R., Khondoker, R., Strekopytov, S., Humphreys-Williams, E., Achterberg, E.P., Rijkenberg, M.J.A., Gerringa, L.J.A., de Baar, H.J.W., 2016. Return of naturally sourced pb to Atlantic surface waters. Nat. Commun. 7 https://doi.org/10.1038/ncomms12921.
Carvalho, L.M.V., Jones, C., Liebmann, B., 2004. The South Atlantic convergence zone: intensity, form, persistence, and relationships with intraseasonal to interannual activity and extreme rainfall. J. Clim. 17 (1), 88–108. https://doi.org/10.1175/1520-0442(2004)017<0088:TSACZI>2.0.CO;2.
Chelton, D.B., Schlax, M.G., Samelson, R.M., 2011. Global observations of nonlinear mesoscale eddies. Prog. Oceanogr. 91 (2), 167–216. https://doi.org/10.1016/j.pocean.2011.01.002.
Chen, M., Boyle, E.A., Lee, J.M., Nurhati, I., Zurbrick, C., Switzer, A.D., Carrasco, G., 2016. Lead isotope exchange between dissolved and fluvial particulate matter: a laboratory study from the Johor River estuary. Philos. Trans. R. Soc. A Math. Phys. Eng. Sci. 374 (2081) https://doi.org/10.1098/rsta.2016.0054.
Chen, M., Carrasco, G., Zhao, N., Wang, X., Lee, J.N., Tanzil, J.T.I., Annammala, K.V., Poh, S.C., Lauro, F.M., Ziegler, A.D., Duangnamon, D., Boyle, E.A., 2023. Boundary exchange completes the marine Pb cycle jigsaw. Proc. Natl. Acad. Sci. U. S. A. 120 (6) https://doi.org/10.1073/pnas.2213163120.
Cindrić, A.M., Garnier, C., Oursel, B., Pižeta, I., Omanović, D., 2015. Evidencing the natural and anthropogenic processes controlling trace metals dynamic in a highly stratified estuary: the Krka River estuary (Adriatic, Croatia). Mar. Pollut. Bull. 94 (1–2), 199–216. https://doi.org/10.1016/j.marpolbul.2015.02.029.
Cochran, J.K., Mckibbin-Vaughan, T., Dornblaser, M.M., Hirschberg, D., Livingston, H. D., Buesseler, K.O., 1990. 210Pb scavenging in the North Atlantic and North Pacific oceans. Earth Planet. Sci. Lett. 332–352.
Curia, D., Duncan, P.M., Grealy, M., McKenna, J., Hill, A., 2018. Microseismic monitoring of vaca muerta completions in the Neuquén Basin,Argentina. Leading Edge 37 (4), 262–269. https://doi.org/10.1190/tle37040262.1.
Da-Allada, C.Y., Jouanno, J., Gaillard, F., Kolodziejczyk, N., Maes, C., Reul, N., Bourlès, B., 2017. Importance of the Equatorial Undercurrent on the sea surface salinity in the eastern equatorial Atlantic in boreal spring. J. Geophys. Res.: Oceans 122 (1), 521–538.
Dai, M.-H., Martin, J.-M., 1995. First data on trace metal level and behaviour in two major Arctic river-estuarine systems (Ob and Yenisey) and in the adjacent Kara Sea, Russia. Earth Planet. Sci. Lett. 131, 127–141.
de Decco, H.T., Torres Junior, A.R., Pezzi, L.P., Landau, L., 2018. Revisiting tropical instability wave variability in the Atlantic Ocean using SODA reanalysis. Ocean Dyn. 68 (3), 327–345. https://doi.org/10.1007/s10236-017-1128-2.
Eichler, A., Gramlich, G., Kellerhals, T., Tobler, L., Schwikowski, M., 2015. Pb pollution from leaded gasoline in South America in the context of a 2000-year metallurgical history. <sb:contribution><sb:title>Sci. </sb:title></sb:contribution><sb:host><sb:issue><sb:series><sb:title>Adv.</sb:title></sb:series></sb:issue></sb:host> 1 (2). https://doi.org/10.1126/sciadv.1400196.
Gaiero, D.M., Probst, J.L., Depetris, P.J., Bidart, S.M., Leleyter, L., 2003. Iron and other transition metals in Patagonian riverborne and windborne materials: geochemical control and transport to the southern South Atlantic Ocean. Geochim. Cosmochim. Acta 67 (19), 3603–3623. https://doi.org/10.1016/S0016-7037(03)00211-4.
Galer, S.J.G., Abouchami, W., 1998. Practical application of lead triple spiking for correction of instrumental mass discrimination. Mineral. Mag. 491–492.
Gassó, S., Stein, A.F., 2007. Does dust from Patagonia reach the sub-Antarctic Atlantic Ocean? Geophys. Res. Lett. 34 (1), 3–7. https://doi.org/10.1029/2006GL027693.
GEOTRACES Intermediate Data Product Group, 2021. The GEOTRACES Intermediate Data Product 2021 (IDP2021). NERC EDS British Oceanographic Data Centre NOC.
Gioia, S.M.C.L., Babinski, M., Weiss, D.J., Kerr, A.A.F.S., 2010. Insights into the dynamics and sources of atmospheric lead and particulate matter in São Paulo, Brazil, from high temporal resolution sampling. Atmos. Res. 98 (2–4), 478–485. https://doi.org/10.1016/j.atmosres.2010.08.016.
Gioia, S.M.C.L., Babinski, M., Weiss, D.J., Spiro, B., Kerr, A.A.F.S., Veríssimo, T.G., Ruiz, I., Prates, J.C.M., 2017. An isotopic study of atmospheric lead in a megacity after phasing out of leaded gasoline. Atmos. Environ. 149, 70–83. https://doi.org/10.1016/j.atmosenv.2016.10.049.
Gordon, A.L., 1989. Brazil-Malvinas confluence - 1984. Deep-Sea Res. 36 (3), 359–384.
Guerzoni, S., Molinaroli, E., Rossini, P., Rampazzo, G., Quarantotro, G., de Falco, G., Cristini, S., 1999. Role of desert aerosol in metal fluxes in the Mediterranean area. Chemosphere 39 (2), 229–246.
Helmers, E., Rutgers van der Loeff, M.M., 1993. Lead and aluminum in Atlantic surface waters (50°N to 50°S) reflecting anthropogenic and natural sources in the eolian transport. J. Geophys. Res. 98 (C11), 20261–20273. https://doi.org/10.1029/93jc01623.
Helmers, E., Mart, L., Schulz-Baldes, M., Ernst, W., 1990. Temporal and spatial variations of lead concentrations in Atlantic surface waters. Mar. Pollut. Bull. 21 (11), 515–518.
Henderson, G.M., Maier-Reimer, E., 2002. Advection and removal of 210Pb and stable Pb isotopes in the oceans: a general circulation model study. Geochim. Cosmochim. Acta 66 (2), 257–272. https://doi.org/10.1016/S0016-7037(01)00779-7.
Hsu, S.C., Lin, F.J., Jeng, W.L., 2005. Seawater solubility of natural and anthropogenic metals within ambient aerosols collected from Taiwan coastal sites. Atmos. Environ. 39 (22), 3989–4001. https://doi.org/10.1016/j.atmosenv.2005.03.033.
Huffman, G.J., Behrangi, A., Bolvin, D.T., Nelkin, E.J., 2021. In: Huffman, G.J., Behrangi, A., Bolvin, D.T., Nelkin, E.J. (Eds.), GPCP Version 3.1 Daily Precipitation Data Set. https://doi.org/10.5067/MEASURES/GPCP/DATA303.
Jickells, T.D., An, Z.S., Andersen, K.K., Baker, A.R., Bergametti, G., Brooks, N., Cao, J.J., Boyd, P.W., Duce, R.A., Hunter, K.A., Kawahata, H., Kubilay, N., Laroche, J., Liss, P. S., Mahowald, N., Prospero, J.M., Ridgwell, A.J., Tegen, I., Torres, R., 2005. Global iron connections between desert dust, ocean biogeochemistry, and climate. Science 308, 67–71. https://doi.org/10.1126/science.1105959.
Johnson, M.S., Meskhidze, N., Solmon, F., Gassó, S., Chuang, P.Y., Gaiero, D.M., Yantosca, R.M., Wu, S., Wang, Y., Carouge, C., 2010. Modeling dust and soluble iron deposition to the South Atlantic Ocean. J. Geophys. Res. Atmos. 115 (15) https://doi.org/10.1029/2009JD013311.
Jones, C., Carvalho, L.M.V., 2002. Active and break phases in the South American monsoon system. J. Clim. 15 (8), 905–914. https://doi.org/10.1175/1520-0442(2002)015<0905:AABPIT>2.0.CO;2.
Kadko, D., Aguilar-Islas, A., Buck, C.S., Fitzsimmons, J.N., Landing, W.M., Shiller, A., Till, C.P., Bruland, K.W., Boyle, E.A., Anderson, R.F., 2020. Sources, fluxes and residence times of trace elements measured during the U.S. GEOTRACES East Pacific Zonal Transect. Mar. Chem. 222 https://doi.org/10.1016/j.marchem.2020.103781.
Kalnay, E., Kanamitsu, M., Kistler, R., Collins, W., Deaven, D., Gandin, L., Iredell, M., Saha, S., White, G., Woollen, J., Zhu, Y., 1996. The NCEP/NCAR 40-year reanalysis project. Bull. Am. Meteorol. Soc. 77 (3), 437–472.
Kelly, A.E., Reuer, M.K., Goodkin, N.F., Boyle, E.A., 2009. Lead concentrations and isotopes in corals and water near Bermuda, 1780–2000. Earth Planet. Sci. Lett. 283 (1–4), 93–100. https://doi.org/10.1016/j.epsl.2009.03.045.
Khondoker, R., Weiss, D., van de Flierdt, T., Rehkämper, M., Kreissig, K., Coles, B.J., Strekopytov, S., Humphreys-Williams, E., Dong, S., Bory, A., Bout-Roumazeilles, V., Smichowski, P., Cid-Agüero, P., Babinski, M., Losno, R., Monna, F., 2018. New constraints on elemental and Pb and Nd isotope compositions of South American and Southern African aerosol sources to the South Atlantic Ocean. Chem. Erde 78 (3), 372–384. https://doi.org/10.1016/j.chemer.2018.05.001.
Klaver, M., Carey, S., Nomikou, P., Smet, I., Athanasios, G., Vroon, P., 2016. A distinct source and differentiation history for kolumbo submarine volcano, Santorini volcanic field,Aegean arc. Geochem. Geophys. Geosyst. 1–26. https://doi.org/10.1002/2016GC006398.Received.
Kodama, Y.-M., 1993. Large-scale common features of sub-tropical convergence zones (the Baiu Frontal Zone, the SPCZ, and the SACZ) part II: conditions of the circulations for generating the STCZs. J. Meteorol. Soc. Jpn. Ser. II 71 (5), 581–610.
Kok, J.F., Adebiyi, A.A., Albani, S., Balkanski, Y., Checa-Garcia, R., Chin, M., Colarco, P. R., Hamilton, D.S., Huang, Y., Ito, A., Klose, M., Leung, D.M., Li, L., Mahowald, N.M., Miller, R.L., Obiso, V., Pérez García-Pando, C., Rocha-Lima, A., Wan, J.S., Whicker, C.A., 2021. Improved representation of the global dust cycle using observational constraints on dust properties and abundance. Atmos. Chem. Phys. 21 (10), 8127–8167. https://doi.org/10.5194/acp-21-8127-2021.
Komárek, M., Ettler, V., Chrastný, V., Mihaljevič, M., 2008. Lead isotopes in environmental sciences: a review. Environ. Int. 34 (4), 562–577. https://doi.org/10.1016/j.envint.2007.10.005.
Kumar, A., Abouchami, W., Galer, S.J.G., Garrison, V.H., Williams, E., Andreae, M.O., 2014. A radiogenic isotope tracer study of transatlantic dust transport from Africa to the Caribbean. Atmos. Environ. 82, 130–143.
Lovei, M., 1996. Phasing Out Lead from Gasoline: World-Wide-Experience and Policy Implications.
Lumpkin, R., Garzoli, S.L., 2005. Near-surface circulation in the Tropical Atlantic Ocean. Deep-Sea Res.Part I: Oceanogr.Res.Pap. 52 (3), 495–518. https://doi.org/10.1016/j.dsr.2004.09.001.
Mañay, N., Cousillas, A.Z., Alvarez, C., Heller, T., 2008. Lead contamination in Uruguay: the "La Teja" neighborhood case. In: Reviews of Environmental Contamination and Toxicology.
Marsan, D., Rigaud, S., Church, T., 2014. Natural radionuclides 210Po and 210Pb in the Delaware and Chesapeake Estuaries: modeling scavenging rates and residence times. J. Environ. Radioact. 138, 447–455. https://doi.org/10.1016/j.jenvrad.2014.08.014.
Metcalf, W.G., Voorhis, A.D., Stalcup, M.C., 1962. The Atlantic equatorial undercurrent. J. Geophys. Res. 67 (6), 2499–2508.
Middag, R., van Hulten, M.M.P., van Aken, H.M., Rijkenberg, M.J.A., Gerringa, L.J.A., Laan, P., de Baar, H.J.W., 2015. Dissolved aluminium in the ocean conveyor of the West Atlantic Ocean: effects of the biological cycle, scavenging, sediment resuspension and hydrography. Mar. Chem. 177, 69–86. https://doi.org/10.1016/j.marchem.2015.02.015.
Niisoe, T., Nakamura, E., Harada, K., Ishikawa, H., Hitomi, T., Watanabe, T., Wang, Z., Koizumi, A., 2010. A global transport model of lead in the atmosphere. Atmos. Environ. 44 (14), 1806–1814. https://doi.org/10.1016/j.atmosenv.2010.01.001.
Nozaki, Y., Thomson, J., Turekian, K.K., 1976. The distribution of 210Pb and 210Po in the surface waters of the Pacific Ocean. Earth Planet. Sci. Lett. 32, 304–312.
Nriagu, J.O., 1979. Global inventory of natural and anthrpogenic emissions of trace metals to the atmosphere. Nature 279, 409–411.
Nriagu, J., Jinabhai, C., Naidoo, R., Coutsoudis, A., 1996. Atmospheric lead pollution in KwaZulu/Natal, South Africa. Sci. Total Environ. 191 (1–2), 69–76.
Nriagu, J.O., Pacyna, J.M., 1988. Quantitative assessment of worldwide contamination of air, water and soils by trace metals. Nature 333, 134–139.

Pacyna, J.M., Pacyna, E.G., 2001. An assessment of global and regional emissions of trace metals to the atmosphere from anthropogenic sources worldwide. Environ. Rev. 9 (4), 269–298. https://doi.org/10.1139/er-9-4-269.

Patterson, C.C., Settle, D.M., 1987. Review of data on eolian fluxes of industrial and natural lead to the lands and seas in remote regions on a global scale. Mar. Chem. 22 (2–4), 137–162. https://doi.org/10.1016/0304-4203(87)90005-3.

Paul, M., Bridgestock, L., Rehkämper, M., van de Flierdt, T., Weiss, D., 2015a. High-precision measurements of seawater Pb isotope compositions by double spike thermal ionization mass spectrometry. Anal. Chim. Acta 863 (1), 59–69. https://doi.org/10.1016/j.aca.2014.12.012.

Paul, M., van de Flierdt, T., Rehkämper, M., Khondoker, R., Weiss, D., Lohan, M.C., Homoky, W.B., 2015b. Tracing the Agulhas leakage with lead isotopes. Geophys. Res. Lett. 42 (20), 8515–8521. https://doi.org/10.1002/2015GL065625.

Peterson, R.G., Stramma, L., 1991. Upper-level circulation in the South Atlantic Ocean. Prog. Oceanogr. 26, 1–73.

Pohl, C., Kattner, G., Schulz-Baldes, M., 1993. Cadmium, copper, lead and zinc on transects through Arctic and Eastern Atlantic surface and deep waters. J. Mar. Syst. 4, 17–29.

Queirolo, E.I., Ettinger, A.S., Stoltzfus, R.J., Kordas, K., 2010. Association of anemia, child and family characteristics with elevated blood lead concentrations in preschool children from Montevideo, Uruguay. Arch. Environ. Occup. Health 65 (2), 94–100. https://doi.org/10.1080/19338240903390313.

Reuer, M.K., Weiss, D.J., 2002. Anthropogenic lead dynamics in the terrestrial and marine environment. Philos. Trans. R. Soc. A Math. Phys. Eng. Sci. 360 (1801), 2889–2904. https://doi.org/10.1098/rsta.2002.1095.

Rigaud, S., Stewart, G., Baskaran, M., Marsan, D., Church, T., 2015. 210Po and 210Pb distribution, dissolved-particulate exchange rates, and particulate export along the North Atlantic US GEOTRACES GA03 section. Deep-Sea Res.Part II: Top.Stud. Oceanogr. 116, 60–78. https://doi.org/10.1016/j.dsr2.2014.11.003.

Rolph, G., Stein, A., Stunder, B., 2017. Real-time Environmental Applications and Display sYstem: READY. Environ. Model. Softw. 95, 210–228. https://doi.org/10.1016/j.envsoft.2017.06.025.

Rosell-Fieschi, M., Pelegrí, J.L., Gourrion, J., 2015. Zonal jets in the equatorial Atlantic Ocean. Prog. Oceanogr. 130, 1–18. https://doi.org/10.1016/j.pocean.2014.08.008.

Rudge, J.F., Reynolds, B.C., Bourdon, B., 2009. The double spike toolbox. Chem. Geol. 265 (3–4), 420–431. https://doi.org/10.1016/j.chemgeo.2009.05.010.

Schlosser, C., Klar, J.K., Wake, B.D., Snow, J.T., Honey, D.J., Woodward, E.M.S., Lohan, M.C., Achterberg, E.P., Mark Moore, C., 2014. Seasonal ITCZ migration dynamically controls the location of the (sub)tropical Atlantic biogeochemical divide. Proc. Natl. Acad. Sci. U. S. A. 111 (4), 1438–1442. https://doi.org/10.1073/pnas.1318670111.

Schlosser, C., Karstensen, J., Woodward, E.M.S., 2019. Distribution of dissolved and leachable particulate Pb in the water column along the GEOTRACES section GA10 in the South Atlantic. Deep-Sea Res.Part I: Oceanogr.Res.Pap. 148, 132–142. https://doi.org/10.1016/j.dsr.2019.05.001.

Schneider, T., Bischoff, T., Haug, G.H., 2014. Migrations and dynamics of the intertropical convergence zone. Nature 513 (7516), 45–53.

Souto-Oliveira, C.E., Babinski, M., Araújo, D.F., Andrade, M.F., 2018. Multi-isotopic fingerprints (Pb, Zn, Cu) applied for urban aerosol source apportionment and discrimination. Sci. Total Environ. 626, 1350–1366. https://doi.org/10.1016/j.scitotenv.2018.01.192.

Stein, A.F., Draxler, R.R., Rolph, G.D., Stunder, B.J.B., Cohen, M.D., Ngan, F., 2015. Noaa's hysplit atmospheric transport and dispersion modeling system. In: Bulletin of the American Meteorological Society, Vol. 96, Issue 12. American Meteorological Society, pp. 2059–2077. https://doi.org/10.1175/BAMS-D-14-00110.1.

Stramma, L., England, M., 1999. On the water masses and mean circulation of the South Atlantic Ocean. J. Geophys. Res. Oceans 104 (C9), 20863–20883. https://doi.org/10.1029/1999jc900139.

Stramma, L., Peterson, R.G., 1990. The South Atlantic Current. J. Phys. Oceanogr. 20 (6), 846–859.

Stramma, L., Schott, F., 1999. The mean flow field of the tropical Atlantic Ocean. Deep-Sea Res.II 46, 279–303.

Todd, H., Todd, D., 2010. Outcome and Influence Evaluation of the UNEP Partnership for Clean Fuels and Vehicles (PCFV).

UNEP, 2021. Era of leaded petrol over, eliminating a major threat to human and planetary health. https://www.unep.org/news-and-stories/press-release/era-leaded-petrol-over-eliminating-major-threat-human-and-planetary.

Urbano, D.F., de Almeida, R.A.F., Nobre, P., 2008. Equatorial undercurrent and North equatorial countercurrent at 38°W: a new perspective from direct velocity data. J. Geophys. Res. Oceans 113 (4). https://doi.org/10.1029/2007JC004215.

van Hulten, M., Middag, R., Dutay, J.C., de Baar, H., Roy-Barman, M., Gehlen, M., Tagliabue, A., Sterl, A., 2017. Manganese in the west Atlantic Ocean in the context of the first global ocean circulation model of manganese. Biogeosciences 14 (5), 1123–1152. https://doi.org/10.5194/bg-14-1123-2017.

Weiss, D., Boyle, E.A., Chavagnac, V., Herwegh, M., Wu, J., 2000. Determination of lead isotope ratios in seawater by quadrupole inductively coupled plasma mass spectrometry after Mg(OH)2 co-precipitation. Spectrochim. Acta B 55, 363–374.

Weiss, D., Boyle, A.B., Wu, J., Chavagnac, V., Michel, A., Reuer, M.K., 2003. Spatial and temporal evolution of lead isotope ratios in the North Atlantic Ocean between 1981 and 1989. J. Geophys. Res. Oceans 108 (10). https://doi.org/10.1029/2000jc000762.

Wilson, D.J., van de Flierdt, T., Adkins, J.F., 2017. Lead isotopes in deep-sea coral skeletons: ground-truthing and a first deglacial Southern Ocean record. Geochim. Cosmochim. Acta 204, 350–374. https://doi.org/10.1016/j.gca.2017.01.052.

Witt, M., Baker, A.R., Jickells, T.D., 2006. Atmospheric trace metals over the Atlantic and South Indian Oceans: Investigation of metal concentrations and lead isotope ratios in coastal and remote marine aerosols. Atmos. Environ. 40 (28), 5435–5451.

Wolff, E.W., Suttie, E.D., 1994. Antarctic snow record of southern hemisphere lead pollution. Geophys. Res. Lett. 21 (9), 781–784.

Xie, R.C., Galer, S.J.G., Abouchami, W., Rijkenberg, M.J.A., de Jong, J., de Baar, H.J.W., Andreae, M.O., 2015. The cadmium-phosphate relationship in the western South Atlantic - the importance of mode and intermediate waters on the global systematics. Mar. Chem. 177, 110–123. https://doi.org/10.1016/j.marchem.2015.06.011.